

TWO DIMENSIONAL OCULOMOTOR PLANT MECHANICAL MODEL
(2DOPMM)

THESIS

Presented to the Graduate Council of
Texas State University–San Marcos
in Partial Fulfillment
of the Requirements

for the Degree

Master of SCIENCE

by

Sampath Jayarathna, B.S.

San Marcos, Texas
August 2010

TWO DIMENSIONAL OCULOMOTOR PLANT MECHANICAL MODEL
(2DOPMM)

Committee Members Approved:

Oleg Komogortsev, Chair

Xiao Chen

Carl Mueller

Approved:

J. Michael Willoughby

Dean of the Graduate College

COPYRIGHT

by

Sampath Jayarathna

2010

ACKNOWLEDGEMENTS

First and foremost, I would like to thank and appreciate my supervisor Dr. Oleg Komogortsev for his continuous support, guidance and supervision throughout my research project. A great part of my research project's success is due to his continuous guidance and critical comments. I also like to offer my sincere thanks to Dr. Xiao Chen and Dr. Carl Mueller for their support and advice as my committee members. I also wish to express my special thanks to Dr. Cecilia Aragon (Lawrence Berkeley National Lab), and Dr. Denise Gobert (Physical Therapy) for their valuable advices and guidance that helped not only for research but also for my personal life. Among our current lab members, I would like to thank Do Hyong Koh, Munikrishne Gowda Sandeep, Evan Dai, and Mahmoud Mechehoul, not only for their help in my research work but also for the precious companionship.

Last but not the least; I would like to thank my wife Nirmala Karunarathna, my baby boy Pahan Jayarathna, for their love, support and encouragement given to me to do my best. Without their continued support and prayers, I could not have successfully completed this project. This work was partially supported by Sigma Xi GIAR program grant, Graduate College/Computer Science travel grants, and Research Enhancement Program (REP) award to Dr. Oleg Komogortsev by the Texas State University-San Marcos.

This manuscript was submitted on June 18th, 2010.

TABLE OF CONTENTS

ACKNOWLEDGEMENTS	v
LIST OF TABLES	vii
LIST OF FIGURES	viii
ABSTRACT	ix
CHAPTER	
I. INTRODUCTION.....	1
II. HUMAN VISUAL SYSTEM.....	6
III. METHODOLOGY.....	41
IV. RESULTS	47
V. CONCLUSION & FUTURE WORK	57
APPENDIX A.....	60
REFERENCES.....	64

LIST OF TABLES

Table	Page
1. Individual Extraocular Muscle Roles	6
2. Sensitivity Rankings	48
3. Neuronal Control Models, $RMSE_{HR}$ and $RMSE_{VR}$	49
4. Neuronal Control Models, $RMSE_{2D}$ and R^2	50

LIST OF FIGURES

Figure	Page
1. Human Eye and Extra-Ocular Muscles.....	2
2. Stationary MEOM of the Agonist Muscle.	9
3. Agonist MEOM.	10
4. Antagonist MEOM.	12
5. The Neuronal Control Signal.	15
6. 2DOPMM: With Four Muscle Forces Responsible for 2D Eye Movements.	20
7. 2DOPMM: Left Downward Rotation, Overview.	21
8. 2DOPMM: Left Downward Rotation.	23
9. 2DOPMM: Horizontal Antagonist Muscle.	25
10. 2DOPMM: Horizontal Agonist Muscle.....	26
11. 2DOPMM: Vertical Agonist Muscle.....	28
12. 2DOPMM: Vertical Antagonist Muscle.	30
13. 2DOPMM: Right Upward Rotation.....	32
14. 2DOPMM: Left Upward Rotation.....	33
15. 2DOPMM: Right Downward Rotation.....	34
16. 2DOPMM: Saccade Invocation Task.	42
17. 1DOPMM: Main Sequence Relationship.	53
18. 2DOPMM: Main Sequence Relationship.	54
19. 1DOPMM: Random Onset/Offset Main Sequence Relationship.....	55
20. 2DOPMM: Random Onset/Offset Main Sequence Relationship.....	56

ABSTRACT

TWO DIMENSIONAL OCULOMOTOR PLANT MECHANICAL MODEL (2DOPMM)

by

Sampath Jayarathna, B.S.

Texas State University–San Marcos

August 2010

SUPERVISING PROFESSOR: OLEG KOMOGORTSEV

This research study builds a two dimensional Oculomotor Plant Mechanical Model (2DOPMM) that is capable of generating eye movement trace and also simulating fixation and saccade eye movement signal on a two dimensional plane. The key difference between the proposed model and the models presented previously is a design that is geared towards linearity and capability of integration into a real-time Human Computer Interaction system while providing force output for each extraocular muscle with values close to physiological measurements. The model is represented as a twelve order system created by a set of linear mechanical components representing major

anatomical properties of extraocular muscles and the eye globe: muscle location, elasticity, viscosity, eye-globe rotational inertia, muscle active state tension, length tension and force velocity relationships. The model is driven by a neuronal control signal and consists of four extraocular muscles (medial, lateral, superior and inferior recti) and an eye globe. Linearity is a key point ensuring a real-time performance in an online implementation of the model with twelve order representation providing close match to the eye anatomical structure.

The goal of the model is to provide an accurate eye position trace during saccades with the duration and main sequence relationships within the physiological capabilities of a normal human. The accuracy of the model is verified against three types of independent eye movement recordings, employing various setups and eye tracker equipment, and 49 subjects. Results indicate that the positional error between the actual and the simulated trajectories is two times smaller than the positional difference between left and right eyes. Practical application of the model lies in the areas requiring the analysis of the eye position trace and properties of the neuronal control signal. Preliminary studies indicate the potential applicability of these types of models in biometrics and in the design of the novel human-computer interaction techniques. A further application of the proposed model exists in the area of extraocular muscle effort estimation and Human Computer Interaction.

CHAPTER I

INTRODUCTION

Human Oculomotor Plant (OP)

Human Oculomotor Plant (OP) consists of six extraocular muscles (medial, lateral, superior, and inferior recti, superior and inferior oblique) and the eye globe. The OP, driven by the neuronal control signal, exhibits six eye movement types: fixations, saccades, smooth pursuits, optokinetic reflex, vestibulo-ocular reflex, and vergence (Leigh & Zee, 2006). Each extraocular muscle is represented by a complex anatomical structure that consists of anatomical components representing such properties as elasticity, viscosity, muscle active state tension, length tension and force velocity relationships. Human eye globe rotates in three degrees of freedom with eye movements following Listing's and Donders's Law (Crawford, Martinez-Trujillo, & Klier, 2003). For normal human's, duration of the saccades is linearly dependent on their amplitude (Carpenter, 1977), in addition, an exponential relationship between saccade amplitude and the maximum velocity exhibited during a saccade is maintained (main-sequence relationship) (Leigh & Zee, 2006).

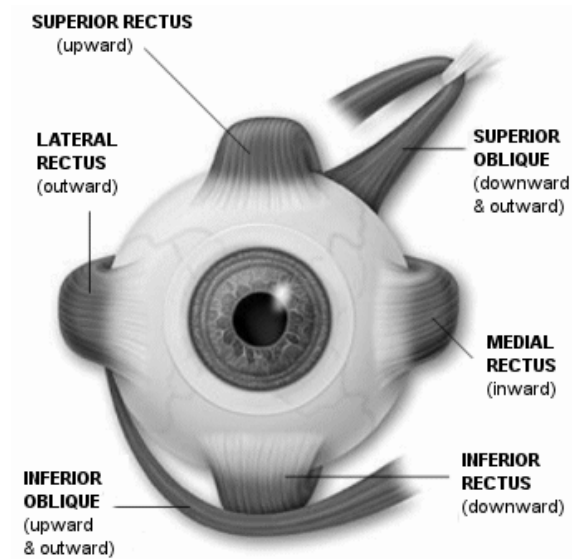


Figure 1. Human Eye and Extra-Ocular Muscles.

Right eye; lateral rectus, medial rectus, superior rectus, inferior rectus, superior oblique and inferior oblique

Oculomotor Plant (OP) Models

There are two categories of the OP models that have been presented to the scientific community so far. The first category is represented by the one dimensional models developed by Westheimer (Westheimer, 1954), Robinson (Robinson, 1973), Clark and Stark (Clark & Stark, 1974), Bahill (Bahill, 1980), Komogortsev & Khan (O. V. Komogortsev & J. Khan, 2009), Martin and Schovanec (Martin & Schovanec, 1998). The model developed by Westheimer modeled the OP as a linear two-order system. Robinson's model added the pulse step neuronal control mechanics with OP system presented as a four-order system. Both models were not capable of producing trajectories that maintained main sequence relationship and represented normal human data. Bahill developed a sixth-order linear homeomorphic OP model, with velocity output close to the

physiological recordings of normal humans. The Bahill's model generated rightward saccades only from the primary eye position. Komogortsev & Khan modified Bahill's model providing the capability of generating both rightward and leftward horizontal saccades from any angular position. The OP model developed by Martin and Schovanec is a non-linear tenth order system, which employs a more anatomically accurate hill-type individual extraocular muscle model with a passive elasticity component modeled in a non linear fashion.

The second category contains three dimensional OP models capable of simulating eye movement trajectory in the 3D space. These models can be broken into two subcategories. The first is represented by the OP models that produce eye positional signal based on the output from the velocity integrator without considering the force output or anatomical properties of the individual extraocular muscles (Raphan, 1998; Tweed, 1997). The second is represented by the models of Polpitiya et al. (Polpitiya, Ghosh, Martin, & Schovanec, 2002) Lockwood-Cooke et al. (Lockwood-Cooke, Martin, & Schovanec, 1999). These OP models are non-linear and provide most accurate representations for the anatomical components such as individual properties of the extraocular muscles and pulley mechanics.

Unfortunately the verification of the models in terms of the correctness of simulated eye movement trajectories is usually performed over a very small pool of subjects (up to three) with exception of (O. V. Komogortsev & J. Khan, 2009), and very frequently it is done manually without numerical verification in terms of the magnitude of the positional error, saccade duration and the properties of the main sequence relationship.

The two dimensional Oculomotor Plant Mathematical Model (2DOPMM) presented in this study builds upon the horizontal OP model created by Komogortsev and Khan (O. Komogortsev, V. & Khan, 2008; O. V. Komogortsev & J. Khan, 2009) (derived from earlier work by Bahill (Bahill, 1980)). The 2DOPMM incorporates several important properties of the human oculomotor plant such as realistic pulse-step properties of the neuronal control signal. Each extraocular muscle is modeled individually, allowing maintaining physiological agonist-antagonist nature of the extraocular movement dynamics. The model of each muscle encapsulates elastic, viscous, active state tension, length tension and force velocity relationships properties by creating a linear mathematical representation of each component.

The goal of the model is to simulate eye positional signal on a two dimensional plane with characteristics resembling normal humans. These characteristics are represented by the difference between simulated and the actual position of the eye movement signal, the relationship between the amplitude and the duration of the saccade and the properties of the main-sequence relationship (dependency of the maximum eye velocity on the amplitude of a saccade). A preliminary version of this work has appeared in (O. V. Komogortsev & Jayarathna, 2008), but did not provide the mathematical equations for all directions of movement on the 2D plane and did not validate the model in terms of physiological human data. This study does both and evaluates four existing models of neuronal control developed by Bahill (Bahill, 1980), Komogortsev and Khan (O. V. Komogortsev & J. Khan, 2009), and (Sylvestre & Cullen, 1999) in addition to a novel, regression based neuronal control.

The strength of the proposed model is its linear design that keeps it simple enough to allow its implementation in the real-time eye gaze aware systems. Twelve differential equations representing the model can be broken into two sets of six equations, each allowing parallel computation of the horizontal and vertical components of movement. We hypothesize that the 2D model will allow to investigate novel schemes of Human Computer Interaction as in (O. V. Komogortsev, Ryu, Do, & Gowda, 2009) and improving the robustness of the biometrics systems as presented in (O. V. Komogortsev, Jayarathna, Aragon, & Mechehoul, 2010).

CHAPTER II

HUMAN VISUAL SYSTEM

The Human Eye and OP Muscle Roles

The eye globe is rotated by six Extraocular Muscles (EOM) with each EOM driven by neuronal control signal generated by the brain. The role of each EOM can be represented by the following table (Leigh & Zee, 2006). This section provides the description for the anatomical apparatus involved in execution of basic eye movement types (fixations, saccades) and brainstem control mechanism responsible for extraocular muscle innervations.

Table 1. Individual Extraocular Muscle Roles			
Muscle	Primary	Secondary	Tertiary
Lateral rectus (LR)	Abduction	N/A	N/A
Medial rectus (MR)	Abduction	N/A	N/A
Inferior rectus (IR)	Depression	Extortion	Abduction
Superior rectus (SR)	Elevation	Intorsion	Abduction
Inferior oblique (IO)	Extortion	Elevation	Abduction
Superior oblique (SO)	Intorsion	Depression	Abduction

The eye globe rotates in its socket through the use of six muscles. These six muscles are the medial and the lateral recti – the muscles mainly responsible for horizontal eye movements; superior and inferior recti – the muscles mainly responsible for vertical eye movements; superior and inferior oblique – the muscles mainly responsible for eye rotations around its primary axis of sight; and vertical eye movements.

The brain sends a neuronal control signal to each muscle to direct the muscle to perform its work. A neuronal control signal is anatomically implemented as a neuronal discharge that is sent through a nerve to a designated muscle from the brain (Sparks, 2002). The frequency of this discharge determines the level of muscle innervations and results in a specific amount of work that a muscle will perform. The neuronal control signal for the vertical and horizontal components of the eye movements is generated by different parts of the brain. Specifically, the premotor neurons in the pons and medulla are responsible for the horizontal movements and rostral midbrain is responsible for the vertical movement. The roles of the individual EOMs can be defined as agonist (subscript notation AG) – the EOM that pulls the eye globe in the required direction and the antagonist (subscript notation ANT) – the EOM that resists the pull. In the Oculomotor Plant several EOMs play the role of agonist with remaining muscles assigned the antagonist roles. The neuronal control signal during saccades resembles a pulse step function where the step part of the signal is determined by the angular eye position prior and after the saccade and pulse part of the signal is determined by the saccadic amplitude. The eye position during the onset of a saccade and the saccade's amplitude and direction define pulse and step parameters of the control signal. Once the parameters of the

neuronal control signal are calculated by the brain, the control signal is sent as a neuronal discharge at the calculated frequency. During eye fixations neuronal discharge is performed at a constant rate that is linearly related to the eye position.

Extraocular Muscle Structure

Each muscle is represented by a complex anatomical structure (Wilkie, 1976). Each EOM has multitude of properties such as: *active state tension* – tension developed as a result of the innervations of a muscle by neuronal control signal, *length tension relationship* – the relationship between the length of a muscle and the force it is capable of exerting, *force velocity relationship* - the relationship between the velocity of a muscle extension/contraction and the force it is capable of exerting, **passive elasticity** – the resisting properties of a muscle not innervated by the neuronal control signal, *series elasticity* – resistive properties of a muscle while the muscle is innervated by the neuronal control signal. More detailed description of these properties can be found in (Bahill, 1980). In addition to the individual muscle properties the eye globe has passive elastic and viscous characteristics due to the properties of the surrounding tissues.

Stationary Model of EOM (MEOM)

Figure 2 presents an eye globe depicted in its primary position (0, 0) in a stationary state with an arbitrary innervated extraocular muscle M attached to the eye globe and an eye socket wall. The EOM is innervated but not extending or shortening. T_M is the force applied by the muscle to the eye globe. N_M is a neuronal control signal supplied to the muscle. F_M is the active state tension inside of the muscle; it is modeled as

an ideal force generator. The series elasticity component is modeled as a linear spring $K_{SE} \cdot \theta_{SE_M}$, where θ_{SE_M} is the displacement of the spring and K_{SE} is the spring's coefficient. The length tension component is modeled as a linear spring that adds its force to the active state tension.

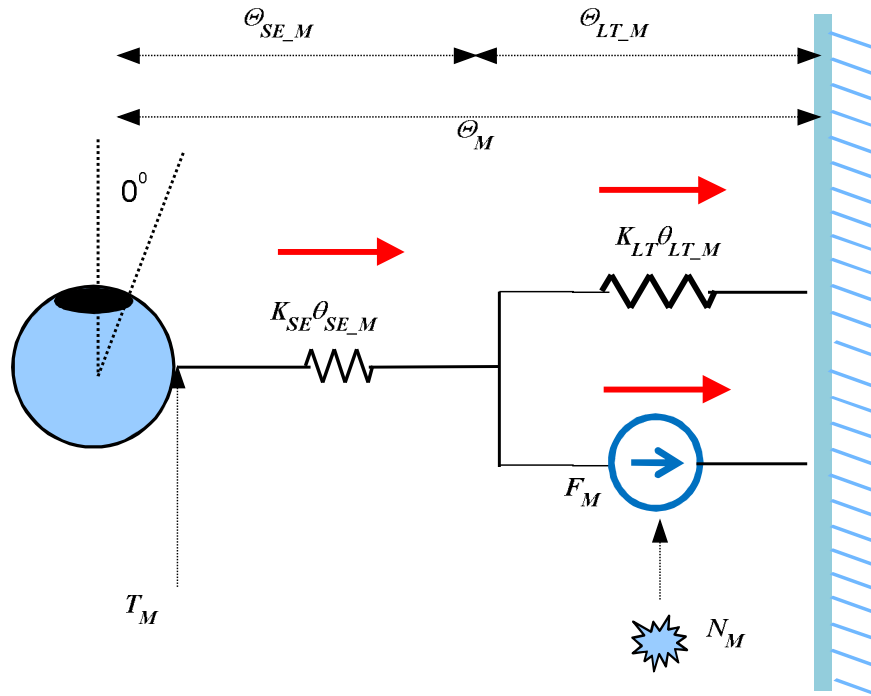


Figure 2. Stationary MEOM of the Agonist Muscle.

The force created by the length tension spring is $K_{LT} \cdot \theta_{LT_M}$, where θ_{LT_M} is the displacement of the spring and K_{LT} is the spring's coefficient. θ_{LT} is the combined displacement of the series elasticity and length tension component $\theta_M = \theta_{LT_M} + \theta_{SE_M}$. In the Model of EOM (MEOM) the active state tension and length tension components move simultaneously.

Agonist EOM Model

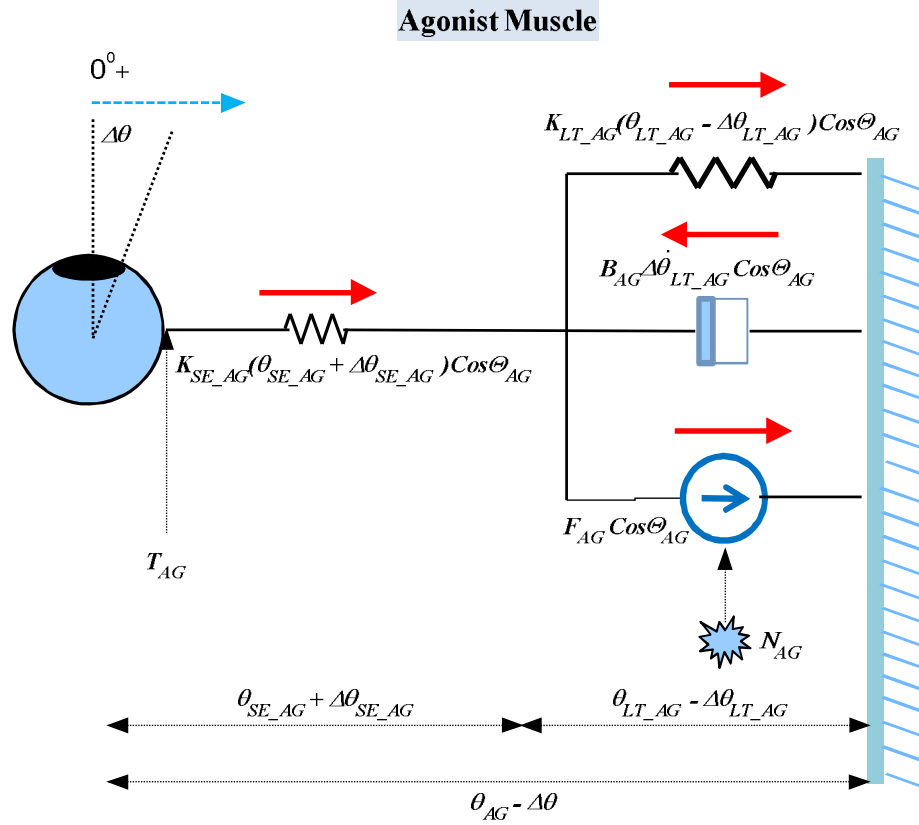


Figure 3. Agonist MEOM.

The agonist muscle contracts, rotates the eye globe and stretches the antagonist muscle. The MEOM of the agonist muscle pulling the eye globe in the direction of displacement $\Delta\theta$ can be presented by Figure 3. The original length of the displacement in the series elasticity spring and the length tension spring added together is θ_{AG} . Considering that the eye globe moves to the direction specified by displacement in $\Delta\theta$ degrees, the original displacement θ_{AG} is reduced making the resulting displacement $\theta_{AG} - \Delta\theta$. The displacement $\Delta\theta$ is $\Delta\theta = \Delta\theta_{SE_AG} - \Delta\theta_{LT_AG}$. Muscle contraction expands the series elastic component making the resulting displacement $\theta_{SE_AG} + \Delta\theta_{SE_AG}$. Muscle contraction

shortens the length tension component making the resulting displacement $\theta_{LT_AG} - \Delta\theta_{LT_AG}$. The damping component modeling the force velocity relationship $B_{AG}\Delta\dot{\theta}_{LT_AG}$ resists the muscle contraction. The amount of resistive force produced by the damping component is based upon the velocity of contraction of the length tension component.

Using Figure 3, we can write the equation of force with which the part of the diagram responsible for contraction (active state tension, damping component, length tension component) pulls the series elasticity component.

$$T_{AG} = F_{AG} + K_{LT}(\theta_{LT_AG} - \Delta\theta_{LT_AG}) - B_{AG}\Delta\dot{\theta}_{LT_AG} \quad (1)$$

Resisting the contraction, the series elasticity component propagates the contractile force by pulling the eye globe with the same force T_{AG} .

$$T_{AG} = K_{SE}(\theta_{SE_AG} + \Delta\theta_{SE_AG}) \quad (2)$$

Equations 1 and 2 can be rearranged to move the contribution of the length tension (θ_{LT_AG}) and series elasticity (θ_{SE_AG}) components to the modified active state tension (\hat{F}_{AG}) and damping components (\hat{B}_{AG}). This transition allows to present force equations with a variable depicting eye globe rotation $\Delta\theta$. Details of this calculations are presented in (Oleg V. Komogortsev, 2007).

$$T_{AG} = \frac{\hat{F}_{AG}K_{SE}}{K_{SE} + K_{LT}} - \frac{\Delta\theta K_{SE}K_{LT}}{K_{SE} + K_{LT}} - \hat{B}_{AG}\Delta\dot{\theta}_{LT_AG} \quad (3)$$

$$T_{AG} = K_{SE}(\Delta\theta_{LT_AG} - \Delta\theta) \quad (4)$$

Antagonist EOM Model

Antagonist Muscle

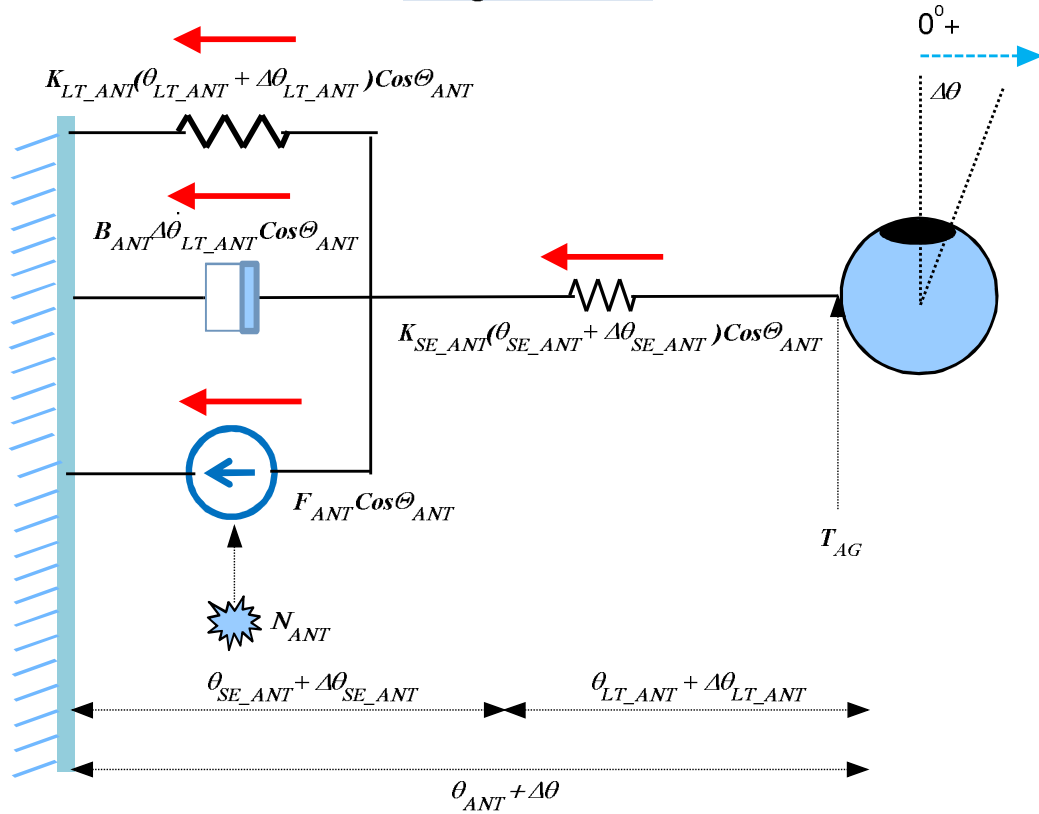


Figure 4. Antagonist MEOM.

The antagonist muscle is stretched by the pull created by the agonist muscles. The MEOM of the antagonist with resulting eye globe displacement of $\Delta\theta$ can be represented by Figure 4. Originally the length of the displacement in the series elasticity and the length tension springs added together is θ_{ANT} . θ_{ANT} increases when the eye moves to the right by $\Delta\theta$, making the resulting displacement $\theta_{ANT} + \Delta\theta$. Both length tension and series elasticity components lengthen as a result of the pull created by the agonist EOMs. The eye rotation $\Delta\theta$ can be split into the displacement of the series elasticity component and

the length tension component: $\Delta\theta = \Delta\theta_{SE_ANT} + \Delta\theta_{LT_ANT}$. The resulting displacement for the series elasticity component is $\theta_{SE_ANT} + \Delta\theta_{SE_ANT}$ and for the length tension component is $\theta_{LT_ANT} + \Delta\theta_{LT_ANT}$. The damping component modeling the force velocity relationship $B_{ANT}\Delta\dot{\theta}_{LT_ANT}$ resists the muscle stretching. The amount of resistive force is based upon the velocity of stretching of the length tension component.

Using Figure 4, we can write the equation of force with which the part of the diagram responsible for the contraction (active state tension, damping component, length tension component) pulls the series elasticity component.

$$T_{ANT} = -F_{ANT} - K_{LT}(\theta_{LT_ANT} - \Delta\theta_{LT_ANT}) - B_{ANT}\Delta\dot{\theta}_{LT_ANT} \quad (5)$$

Resisting the contraction the series elasticity component propagates the contractile force by pulling the eye globe with the same force T_{ANT} .

$$T_{ANT} = K_{SE}(\theta_{SE_ANT} + \Delta\theta_{SE_ANT}) \quad (6)$$

Equations (5) and (6) can be used to calculate the force T_{ANT} in terms of the eye rotation $\Delta\theta$, and displacement $\Delta\theta_{LT_ANT}$ in the length tension component of the muscle.

Details of this calculations are presented in (Oleg V. Komogortsev, 2007).

$$T_{ANT} = -\frac{\hat{F}_{ANT}K_{SE}}{K_{SE} + K_{LT}} - \frac{\Delta\theta K_{SE}K_{LT}}{K_{SE} + K_{LT}} - \hat{B}_{ANT}\Delta\dot{\theta}_{LT_ANT} \quad (7)$$

$$T_{ANT} = -K_{SE}(\Delta\theta - \Delta\theta_{LT_ANT}) \quad (8)$$

Neuronal control of the Agonist and Antagonist EOMs

The neuronal control signal is represented as neuronal discharge from the brain, with discharge frequency determining the neuronal innervations of an EOM (Sparks, 2002).

The neuronal discharge during fixations for both agonist $N_{AG_fix}(\theta)$ and antagonist $N_{ANT_fix}(\theta)$ muscles is done at a constant rate with frequency of such discharge determined by the eye angular position θ .

The neuronal control signal during saccades is a pulse-step function. The step part of the signal is created by positional command (angular eye position prior to and after a saccade) and pulse part of the signal is created by the velocity command, which is determined by the amplitude of the programmed saccade.

$$N_{AG_sac}(t) = \begin{cases} N_{AG_sac_onset}, & t_{sac_onset} \leq t < t_{AG_sac_pulse_start} \\ N_{AG_sac_pulse}, & t_{AG_sac_pulse_start} \leq t < t_{AG_sac_pulse_end} \\ N_{AG_sac_offset}, & t_{AG_sac_pulse_end} \leq t < t_{sac_offset} \end{cases}$$

$$N_{ANT_sac}(t) = \begin{cases} N_{ANT_sac_onset}, & t_{sac_onset} \leq t < t_{ANT_sac_pulse_start} \\ N_{ANT_sac_pulse}, & t_{ANT_sac_pulse_start} \leq t < t_{ANT_sac_pulse_end} \\ N_{ANT_sac_offset}, & t_{ANT_sac_pulse_end} \leq t < t_{sac_offset} \end{cases}$$

t_{name} constants present time parameters for each type of muscle and action phase. t is the time elapsed from the beginning of the saccade. Quantity $t_{sac_offset} - t_{sac_onset}$ is referred to as a width of saccade pulse. Figure 5 presents an example of the neuronal control signal for the agonist muscle in case of the 20° horizontal rightward saccade.\

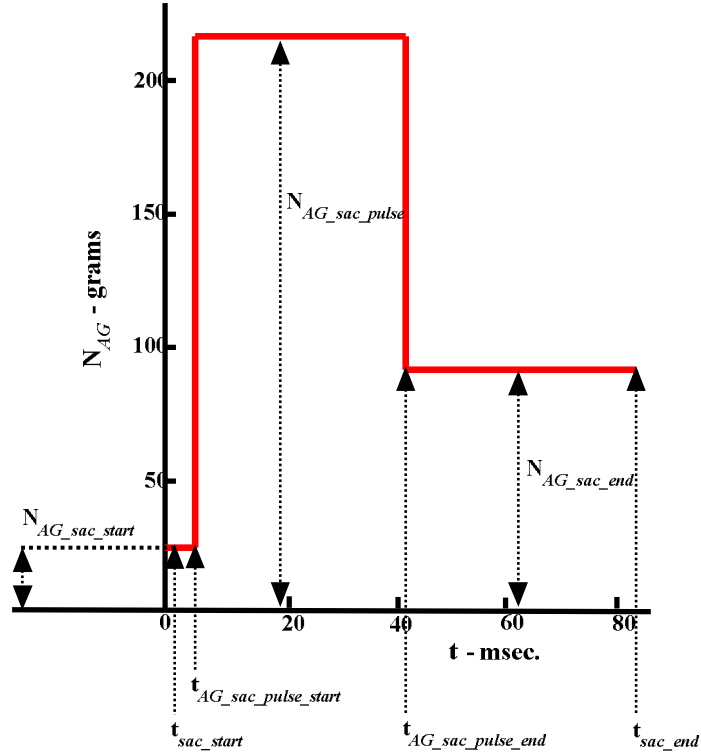


Figure 5. The Neuronal Control Signal.

N_{AG} for the Agonist Muscle for a 20° Rightward Saccade.

Assuming that the eye movement type prior to and after the simulated saccade is a fixation, the equations for the neuronal control signal for the onset and the offset of a saccade can be written as follows:

$$N_{AG_sac_onset}(\theta_{sac_onset}) = \begin{cases} N_{AG_fix}(\theta_{sac_onset}), & \text{if } AG \text{ prior to saccade} \\ N_{ANT_fix}(\theta_{sac_onset}), & \text{if } ANT \text{ prior to saccade} \end{cases}$$

$$N_{AG_sac_offset}(\theta_{sac_offset}) = \begin{cases} N_{AG_fix}(\theta_{sac_offset}), & \text{if } AG \text{ after saccade} \\ N_{ANT_fix}(\theta_{sac_offset}), & \text{if } ANT \text{ after saccade} \end{cases}$$

$$N_{ANT_sac_onset}(\theta_{sac_onset}) = \begin{cases} N_{AG_fix}(\theta_{sac_onset}), & \text{if AG prior to saccade} \\ N_{ANT_fix}(\theta_{sac_onset}), & \text{if ANT prior to saccade} \end{cases}$$

$$V_{ANT_sac_offset}(\theta_{sac_offset}) = \begin{cases} N_{AG_fix}(\theta_{sac_offset}), & \text{if AG after to saccade} \\ N_{ANT_fix}(\theta_{sac_offset}), & \text{if ANT after to saccade} \end{cases}$$

Transformation of the Neuronal Control to Active State Tension

The change of the discharge frequency specified by the neuronal control signal is instantaneous. The change in the active state tension and EOM forces is not. This occurs due to the fact that the spreading of the neuronal control signal is limited by: synchronization variations, synaptic transmission delays, motoneuronal firing frequency acceleration, neuronal conduction velocity, depolarization, spread of activity in the sarcoplasmic reticular formation. The rate of the neuronal control signal is affected by: synaptic transmissions, release and reuptake of the Ca⁺⁺, modification of the actin-myosin fibers (Bahill, 1980).

The active state tension of the agonist and the antagonist go through a low pass filtering process and can be modeled by the following equations:

$$\dot{\hat{F}}_{AG}(t) = \frac{N_{AG} - \hat{F}_{AG}(t)}{\tau_{AG}} \quad (9)$$

$$\dot{\hat{F}}_{ANT}(t) = \frac{N_{ANT} - \hat{F}_{ANT}(t)}{\tau_{ANT}} \quad (10)$$

where τ_{AG} , τ_{ANT} are functions that define the low pass filtering process.

$$\tau_{AG}(t) = \begin{cases} \tau_{AG_sac_de}, & t_{sac_onset} \leq t < t_{AG_sac_pulse_start} \\ \tau_{AG_sac_act}, & t_{AG_sac_pulse_start} \leq t < t_{AG_sac_pulse_end} \\ \tau_{AG_sac_de}, & t_{AG_sac_pulse_end} \leq t < t_{sac_offset} \end{cases}$$

$$\tau_{ANT}(t) = \begin{cases} \tau_{ANT_sac_de}, & t_{sac_onset} \leq t < t_{ANT_sac_pulse_start} \\ \tau_{ANT_sac_act}, & t_{ANT_sac_pulse_start} \leq t < t_{ANT_sac_pulse_end} \\ \tau_{ANT_sac_de}, & t_{ANT_sac_pulse_end} \leq t < t_{sac_offset} \end{cases}$$

$\tau_{AG_sac_act}$, $\tau_{AG_sac_de}$, $\tau_{ANT_sac_act}$, $\tau_{ANT_sac_de}$ are activation/deactivation time constants that define the low pass filtering process.

1D Oculomotor Plant Mathematical Model (1DOPMM)

The equations for the one dimensional case, e.g. horizontal movement, are created by considering all forces that contribute to the rotation of the eye globe.

The agonist force dynamics can be described by combining equations (3), and (4)

$$K_{SE}(\Delta\theta_{LT_AG} - \Delta\theta) = \frac{\hat{F}_{AG}K_{SE}}{K_{SE} + K_{LT}} - \frac{\Delta\theta K_{SE}K_{LT}}{K_{SE} + K_{LT}} - \hat{B}_{AG}\Delta\dot{\theta}_{LT_AG} \quad (11)$$

The antagonist dynamics is derived by combining equations (7), and (8).

$$K_{SE}(\Delta\theta - \Delta\theta_{LT_ANT}) = \frac{\hat{F}_{ANT}K_{SE}}{K_{SE} + K_{LT}} + \frac{\Delta\theta K_{SE}K_{LT}}{K_{SE} + K_{LT}} + \hat{B}_{ANT}\Delta\dot{\theta}_{LT_ANT} \quad (12)$$

Newton's second law is applied to receive the equation connecting the acceleration of the eye globe and inertia to all forces acting on the eye globe

$$J\Delta\ddot{\theta} = T_{AG} + T_{ANT} + K_p\Delta\theta + B_p\Delta\dot{\theta} \quad (13)$$

T_{AG} is the force applied by the agonist muscle to the eye globe, T_{ANT} is the force applied by the antagonist muscle to the eye globe, $K_p\Delta\theta$ is a linear spring that represents the passive elastic properties of the EOMs and the eye globe, $B_p\Delta\dot{\theta}$ is a damping component representing the viscous properties of the eye orbit and surrounding tissues.

Two equations describe the dynamics of the active state tension

$$\dot{\hat{F}}_{AG}(t) = \frac{N_{AG} - \hat{F}_{AG}(t)}{\tau_{AG}} \quad (14)$$

$$\dot{\hat{F}}_{ANT}(t) = \frac{N_{ANT} - \hat{F}_{ANT}(t)}{\tau_{ANT}} \quad (15)$$

The last equation connects the derivative of position to the velocity of the movement signal.

$$\Delta\dot{\theta} = \Delta\dot{\theta} \quad (16)$$

Six differential equations (11)-(16) can be presented in a matrix form with following variables creating a state vector: $x_1(k) = \Delta\theta$ – eye rotation, $x_2(k) = \Delta\theta_{LT_AG}$ and $x_3(k) = \Delta\theta_{LT_ANT}$ – displacement of the length tension component for the agonist and antagonist EOMs respectively, $x_4(k) = \Delta\dot{\theta}$ – eye velocity, $x_5(k) = \hat{F}_{AG}$ and $x_6(k) = \hat{F}_{ANT}$ active state tension for agonist and antagonist muscles.

$$\dot{x} = Ax + u \quad (17)$$

Where x, \dot{x}, u are 1x6 vectors, transition matrix A is a square 6x6 matrix.

$$\begin{pmatrix} 1 & 0 & 0 & \Delta\rho & 0 & 0 \\ \Delta\rho \frac{K_{SE}^2}{(K_{LT} + K_{SE})\hat{B}_{AG}} & \left(1 - \Delta\rho \frac{K_{SE}}{\hat{B}_{AG}}\right) & 0 & 0 & \Delta\rho \frac{K_{SE}}{(K_{LT} + K_{SE})\hat{B}_{AG}} & 0 \\ \Delta\rho \frac{K_{SE}^2}{(K_{LT} + K_{SE})\hat{B}_{ANT}} & 0 & \left(1 - \Delta\rho \frac{K_{SE}}{\hat{B}_{ANT}}\right) & 0 & 0 & -\Delta\rho \frac{K_{SE}}{(K_{LT} + K_{SE})\hat{B}_{ANT}} \\ -\Delta\rho \frac{2K_{SE} + K_p}{J} & \Delta\rho \frac{K_{SE}}{J} & \Delta\rho \frac{K_{SE}}{J} & 1 - \Delta\rho \frac{B_p}{J} & 0 & 0 \\ 0 & 0 & 0 & 0 & \left(1 - \frac{\Delta\rho}{\tau_{AG}}\right) & 0 \\ 0 & 0 & 0 & 0 & 0 & \left(1 - \frac{\Delta\rho}{\tau_{ANT}}\right) \end{pmatrix}$$

u is a vector containing neuronal control signal

$$u_k = \left[0 \quad 0 \quad 0 \quad 0 \quad \frac{\Delta\rho}{\tau_{AG}} N_{AG_sac} \quad \frac{\Delta\rho}{\tau_{ANT}} N_{ANT_sac} \right]^T$$

Equation (17) completely describes the Oculomotor Plant mechanical model during 1D saccades. More detailed description of the 1D case can be found in (O. Komogortsev, V. & Khan, 2008; Oleg V. Komogortsev, 2007).

2D Oculomotor Plant Mathematical Model (2DOPMM)

One of the objectives of the 2DOPMM presented in this study is to accurately simulate saccade trajectories on the 2D plane. According to the data presented in the Table I the rotation of the eye globe with a mapped gaze position on a 2D plane can be primarily attributed to four EOMs – lateral, medial, superior and inferior recti.

The 2DOPMM is consist of four contour points, each with eye muscle attached to eye globe which provides forces to rotate eye globe around the socket through the use of four muscles, lateral rectus, superior rectus, medial rectus and inferior rectus. The subscript notation will identify with LR the parameters that belong to the lateral rectus, with MR the parameters that belong to the medial rectus, with SR the parameters that belong to the superior rectus and IR the parameters that belong to the inferior rectus. Parameters without those subscripts are identical to both types of muscles. The Figure 6 illustrates the eye in the coordination position (0, 0) with respect to the eye center axis in the rest position, with muscles compensate the reactions of each muscle and stabilize the eye in the coordination framework.

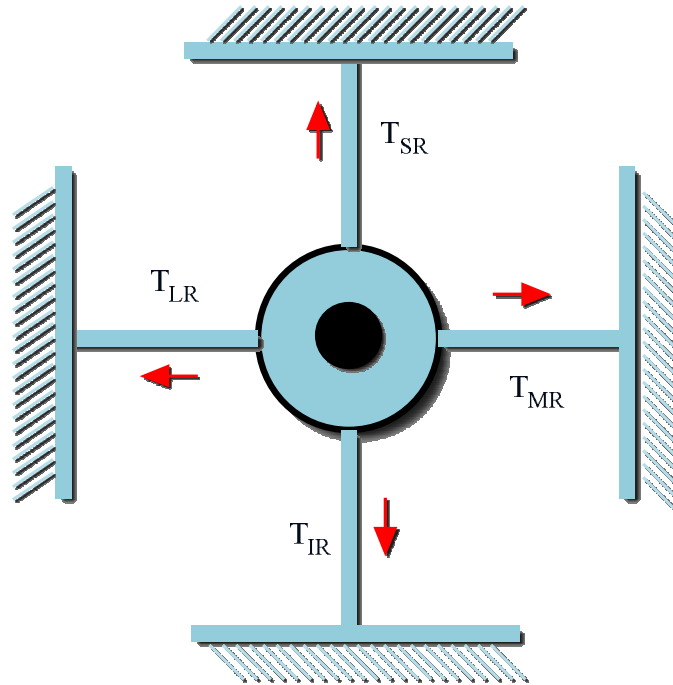


Figure 6. 2DOPMM: With Four Muscle Forces Responsible for 2D Eye Movements.

Each of the following section is modeled based on the role that each muscle plays in a particular situation. As an example when the eye globe moves to the direction of upper right direction, the lateral/superior recti support for the movement and medial/inferior recti resist the movement based on the role of the muscle at that instance. Lateral/superior plays the agonist and medial/inferior plays the antagonist role in this particular situation. Evoked by muscle movement, an eye can move in eight different directions : Right horizontal, Left horizontal, Top vertical, Bottom vertical, Right upward, Left upward, Right downward and Left downward. When eye moves to a particular position from the coordination position (0, 0) as one of eight basic movement types listed above, each muscle connected to the eye globe contract or stretch accordingly.

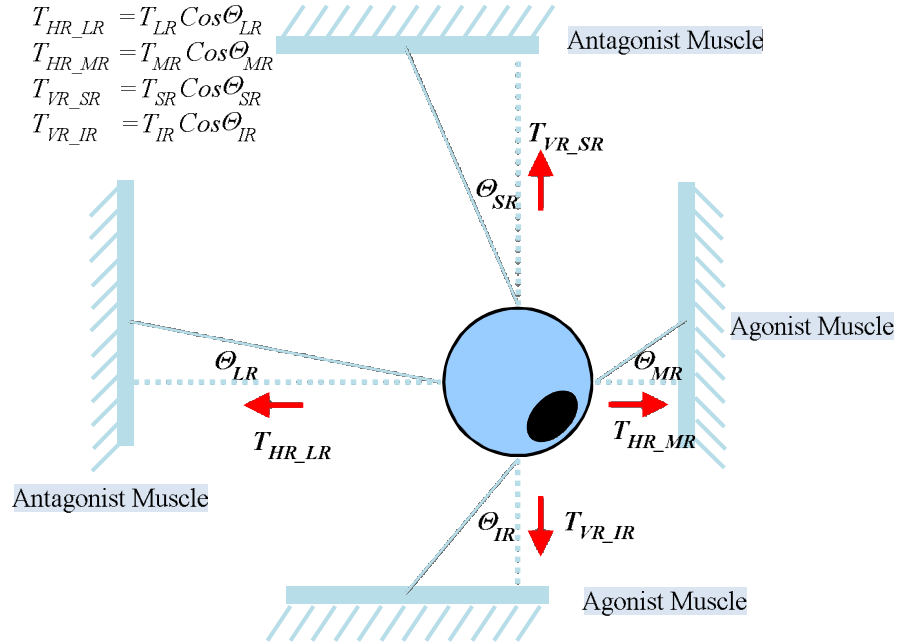


Figure 7. 2DOPMM: Left Downward Rotation, Overview.

Figure 7 depicts the diagram of the model with four EOM's forces (T_{LR} , T_{MR} , T_{SR} , and T_{IR}) responsible for the left downward rotation of the eye globe. In a 2D case EOM movement dynamics and roles remain essentially the same as in 1D case, i.e., the agonist muscles contract and pull the eye globe in the required direction and the antagonist muscles stretch and resist the pull.

Twelve differential equations describe the 2DOPMM. Two equations are created as a result of the application of the Newton's second law to the vertical and the horizontal component of the eye movement. Four equations describe the dynamics of the EOM forces that move the eye globe. Horizontal (subscript notation HR) component of movement is conducted by the forces created by the lateral (T_{HR_LR}) and medial recti (T_{HR_MR}). Vertical (VR) component of movement is conducted by the forces created by

the superior (T_{HR_SR}) and inferior recti (T_{HR_IR}). Four equations describe the transformation of the neuronal control signal in each EOM to the active state tension following the mechanism described in Neuronal Control Signal section. Two equations connect the velocity of the eye movement to the position of the eye in the vertical and horizontal plane.

The derivation of all equations, except the four equations describing the dynamics of the EOM forces, is straight forward and follows the mechanics described in 1DOPMM section. To provide better analytical tractability of the dynamics of the EOM forces following sections present a detailed description of the forces for all four EOMs in case of the four directions of movement: Right upward, Left upward, Right downward, and Left downward. These directions describe all possible scenarios of rotation. The derivation of the 2DOPMM equations for the Right upward is provided in detail. For the remaining cases summary of derivations is provided.

The EOM forces responsible for the eye globe rotation can be found as projections to the horizontal and vertical axis. Figure 8 presents the diagram.

Left Downward Rotation

During the Left Downward movement (saccade between two fixation points) of the right eye the medial rectus and the inferior rectus as agonists move the eye to its destination stretching the antagonist EOMs, lateral and superior recti. $\Delta\theta_{HR}$ represents horizontal component of eye globe rotation measured in degrees while $\Delta\theta_{VR}$ represents vertical component. All EOMs in the 2DOPMM become tilted to a set of new angles θ_{LR} .

θ_{SR} , θ_{MR} , and θ_{IR} in regard to the primary eye globe position. Dynamics of forces in each MEOM are described next.

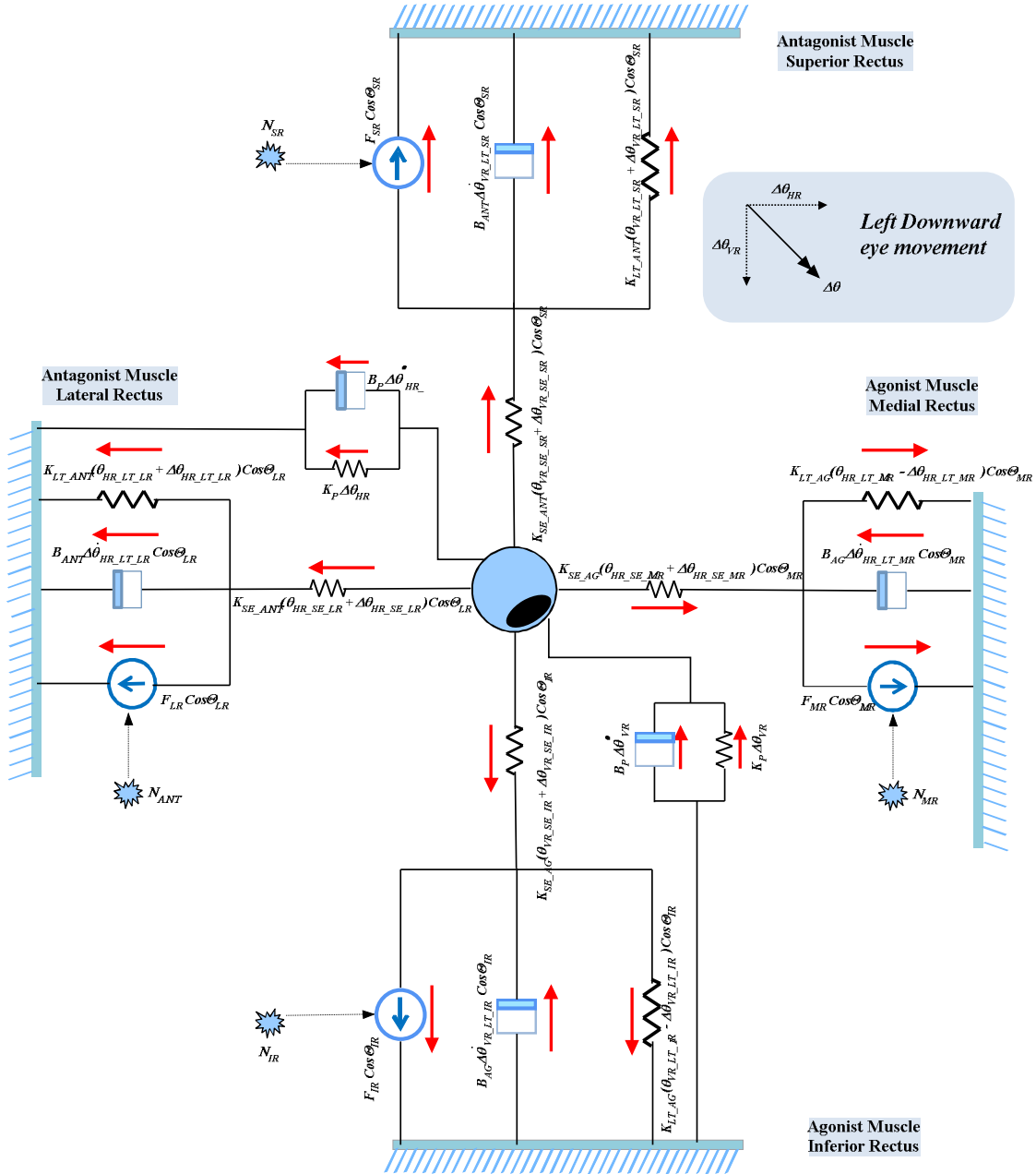


Figure 8. 2DOPMM: Left Downward Rotation.

Detailed Representation of the All Four Muscle Models

Lateral Rectus

The length of the displacement in the series elasticity and the length tension spring components in the horizontal direction added together, prior to rotation, was θ_{HR_LR} . Considering that the right eye moves to the left by $\Delta\theta_{HR}$ the original θ_{HR_LR} displacement in the lateral rectus is increased making the resulting displacement $\theta_{HR_LR} + \Delta\theta_{HR_LR}$. The displacement $\Delta\theta_{HR_LR}$ can be broken into the displacements inside of the series elastic and the length tension components as: $\Delta\theta_{HR_LR} = \Delta\theta_{HR_SE_LR} + \Delta\theta_{HR_LT_LR}$. Both length tension and series elasticity components lengthen as a result of the agonist pull by the horizontal force. Muscle contraction expands the series elastic component making the resulting displacement $\theta_{HR_SE_LR} + \Delta\theta_{HR_SE_LR}$ and lengthens the length tension component making the resulting displacement $\theta_{HR_LT_LR} + \Delta\theta_{HR_LT_LR}$. The damping component modeling the force velocity relationship $B_{ANT}\Delta\dot{\theta}_{HR_LT_LR}$ resists the muscle contraction. The amount of resistive force produced by the damping component is based upon the velocity of contraction of the length tension component.

Using Figure 9, we can write the equation of force with which the part of the diagram responsible for contraction by the lateral rectus (active state tension, damping component, length tension component) pulls the series elasticity component.

$$T_{HR_LR} = F_{LR} \cos \theta_{LR} + K_{LT}(\theta_{HR_LT_LR} + \Delta\theta_{HR_LT_LR}) \cos \theta_{LR} \quad (18)$$

$$+ B_{ANT}\Delta\dot{\theta}_{HR_LT_LR} \cos \theta_{LR}$$

Resisting the contraction, the series elasticity component of lateral rectus propagates the contractile force to the eye globe contributing to the accumulated force T_{HR_LR} .

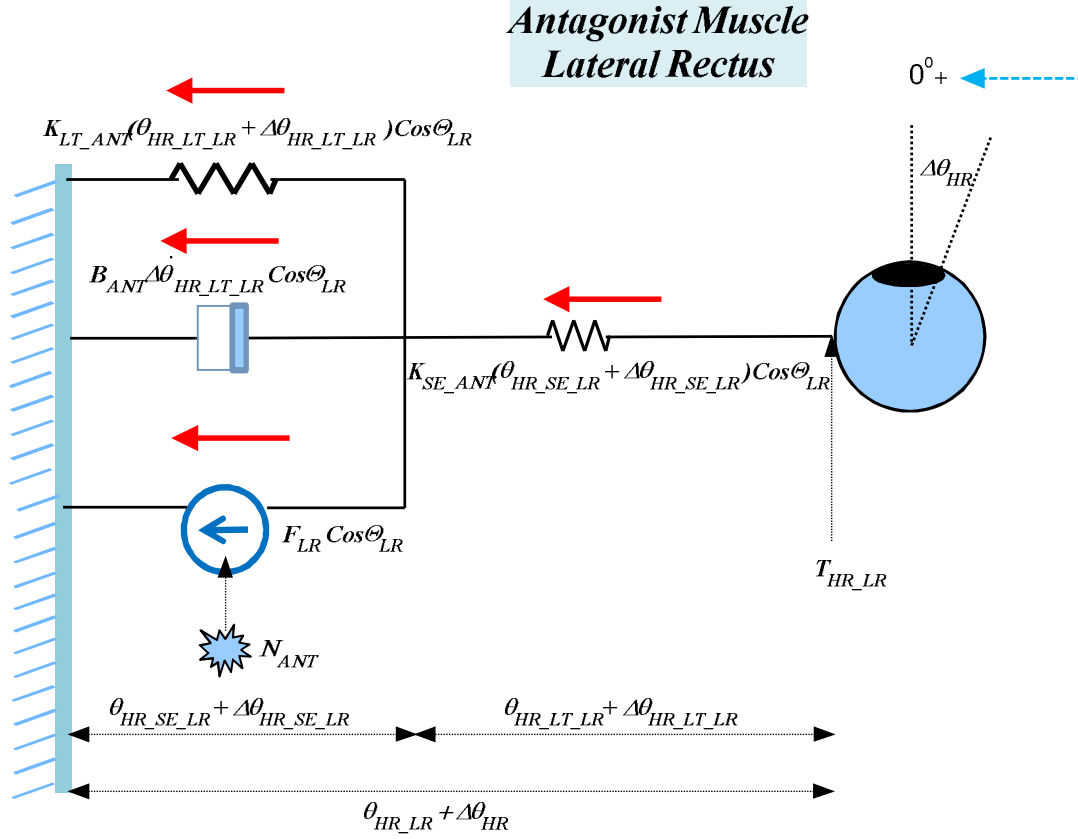


Figure 9. 2DOPMM: Horizontal Antagonist Muscle.

$$T_{HR_LR} = K_{SE}(\theta_{HR_SE_LR} + \Delta\theta_{HR_SE_LR}) \cos \theta_{LR} \quad (19)$$

Equations (18), and (19), can be used to calculate the force T_{HR_LR} in terms of the eye rotation $\Delta\theta_{HR}$ and displacement $\Delta\theta_{HR_LT_LR}$ of the length tension component of the lateral recti EOM. Details of this calculations are presented in Appendix A-1.

$$T_{HR_LR} = \frac{\hat{F}_{LR}K_{SE}}{K_{SE} + K_{LT}} + \frac{\Delta\theta_{HR}K_{SE}K_{LT}}{K_{SE} + K_{LT}} + \hat{B}_{ANT}\Delta\dot{\theta}_{HR_LT_LR} \quad (20)$$

$$\text{Where, } \hat{F}_{LR} = F_{LR} - K_{SE}(\theta_{HR_LR} - \theta_{HR_LT_LR}) + K_{LT}\theta_{HR_LT_LR}$$

$$T_{HR_LR} = K_{SE}(\Delta\theta_{HR} - \Delta\theta_{HR_LT_LR}) \quad (21)$$

Medial Rectus

Prior to the eye's rotation, the length of the displacement in the series elasticity and the length tension springs added together is θ_{HR_MR} . Horizontal eye rotation by $\Delta\theta_{HR}$ degrees causes change in the displacement θ_{HR_MR} by increasing it by $\Delta\theta_{HR_MR}$ making the resulting displacement $\theta_{HR_MR} + \Delta\theta_{HR_MR}$. Muscle contraction expands the series elastic component, making the resulting displacement $\theta_{HR_SE_MR} + \Delta\theta_{HR_SE_MR}$, and shortens the length tension component making the resulting displacement $\theta_{HR_LT_MR} - \Delta\theta_{HR_LT_MR}$. $\Delta\theta_{HR_MR}$ can be split into the displacement of the series elasticity and the length tension components: $\Delta\theta_{HR_MR} = \Delta\theta_{HR_SE_MR} - \Delta\theta_{HR_LT_MR}$.

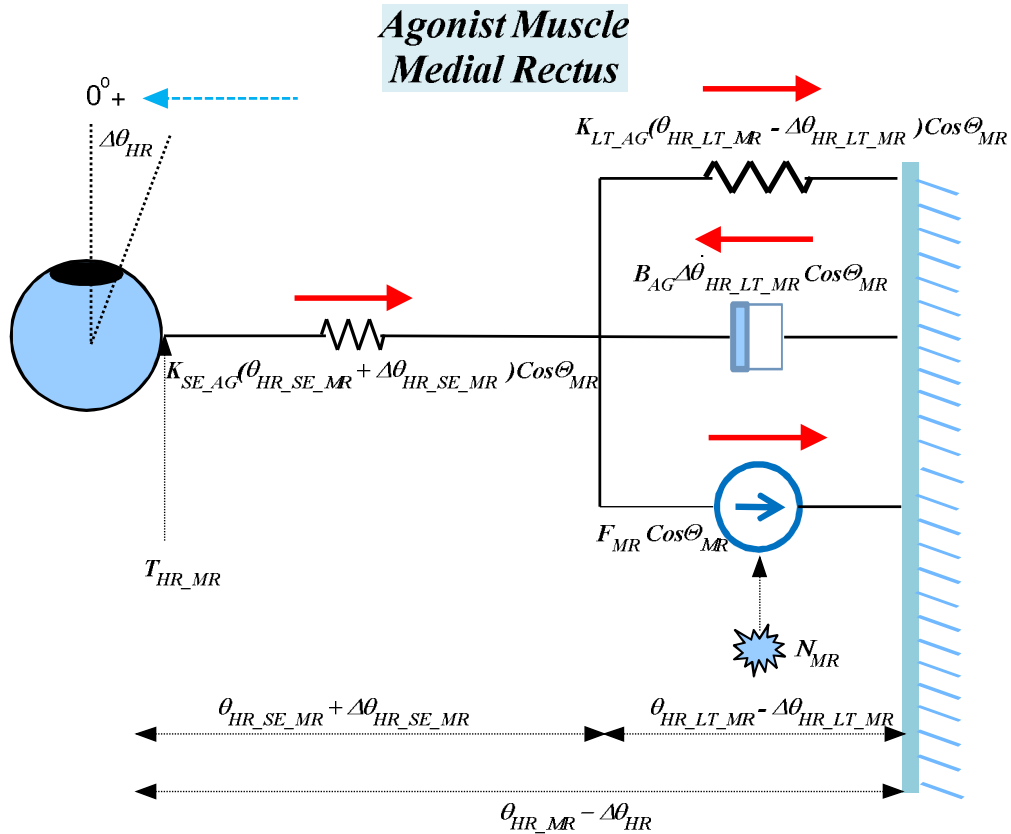


Figure 10. 2DOPMM: Horizontal Agonist Muscle.

Using Figure 10 following equations are obtained:

$$T_{HR_MR} = -F_{MR} \cos \theta_{MR} - K_{LT}(\theta_{HR_LT_MR} - \Delta\theta_{HR_LT_MR}) \cos \theta_{MR} \quad (22)$$

$$+ B_{AG}\Delta\dot{\theta}_{HR_LT_MR} \cos \theta_{MR}$$

$$T_{HR_MR} = -K_{SE}(\theta_{HR_SE_MR} + \Delta\theta_{HR_SE_MR}) \cos \theta_{MR} \quad (23)$$

and

$$T_{HR_MR} = -\frac{\hat{F}_{MR}K_{SE}}{K_{SE} + K_{LT}} + \frac{\Delta\theta_{HR}K_{SE}K_{LT}}{K_{SE} + K_{LT}} + \hat{B}_{AG}\Delta\dot{\theta}_{HR_LT_MR} \quad (24)$$

$$T_{HR_MR} = -K_{SE}(\Delta\theta_{HR_LT_MR} - \Delta\theta_{HR}) \quad (25)$$

where $\hat{F}_{MR} = F_{MR} + K_{SE}\theta_{HR_LT_MR} - K_{SE}\theta_{HR_MR} + K_{LT}\theta_{HR_LT_MR}$.

Details of this calculations are presented in Appendix A-2.

Inferior Rectus

As a result of the vertical eye rotation by $\Delta\theta_{VR}$ degrees, the original displacement θ_{VR_IR} is reduced to $\theta_{VR_IR} - \Delta\theta_{IR}$. The displacement $\Delta\theta_{IR}$ can be broken into $\Delta\theta_{IR} = \Delta\theta_{VR_SE_IR} - \Delta\theta_{VR_LT_IR}$. Muscle contraction expands the series elastic component making the resulting displacement $\theta_{VR_SE_IR} + \Delta\theta_{VR_SE_IR}$. Muscle contraction shortens the length tension component making the resulting displacement $\theta_{VR_LT_IR} - \Delta\theta_{VR_LT_IR}$. The damping component $B_{AG}\Delta\dot{\theta}_{VR_LT_IR}$ resists the muscle contraction.

Using Figure 11 following equations are obtained:

$$T_{VR_IR} = -F_{IR} \cos \theta_{IR} - K_{LT}(\theta_{VR_LT_IR} - \Delta\theta_{VR_LT_IR}) \cos \theta_{IR} \quad (26)$$

$$+ B_{AG}\Delta\dot{\theta}_{VR_LT_IR} \cos \theta_{IR}$$

$$T_{VR_IR} = -K_{SE}(\theta_{VR_SE_IR} + \Delta\theta_{VR_SE_IR}) \cos\theta_{IR} \quad (27)$$

these two equations can be re-arranged as:

$$T_{VR_IR} = -\frac{\hat{F}_{IR}K_{SE}}{K_{SE} + K_{LT}} + \frac{\Delta\theta_{VR}K_{SE}K_{LT}}{K_{SE} + K_{LT}} + \hat{B}_{AG}\Delta\dot{\theta}_{VR_LT_IR} \quad (28)$$

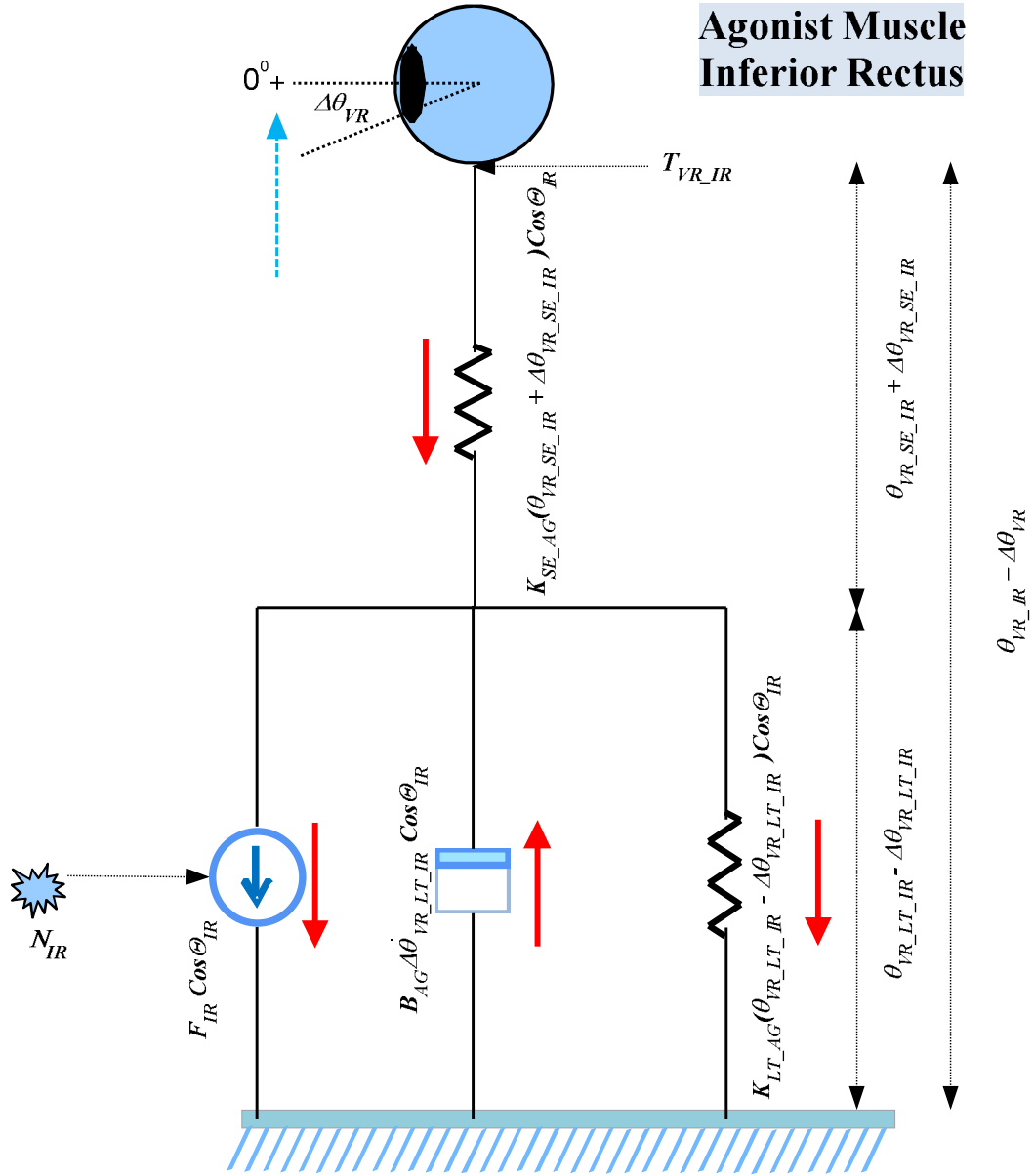


Figure 11. 2DOPMM: Vertical Agonist Muscle.

$$T_{VR_SR} = K_{SE}(\Delta\theta_{VR} - \Delta\theta_{VR_LT_SR}) \quad (29)$$

$$\text{where, } \hat{F}_{SR} = \hat{F}_{SR} + K_{LT}\Delta\theta_{VR_LT_SR} + B_{ANT}\Delta\dot{\theta}_{VR_LT_SR}$$

Details of this calculations are essentially the same as of Medial recuts presented in Appendix A-2 with the values applied in the vertical directions.

Superior Rectus

The behavior of the Superior Rectus is similar to the behaviour of the Lateral Rectus and can be inferred from Figure 12. Resulting equations can be presented as

$$T_{VR_SR} = -F_{SR} \sin \theta_{SR} - K_{LT}(\theta_{VR_LT_SR} - \Delta\theta_{VR_LT_SR}) \sin \theta_{SR} \quad (30)$$

$$+ B_{AG}\Delta\dot{\theta}_{VR_LT_SR} \sin \theta_{SR}$$

$$T_{VR_SR} = -K_{SE}(\theta_{VR_SE_SR} + \Delta\theta_{VR_SE_SR}) \sin \theta_{SR} \quad (31)$$

and

$$T_{VR_SR} = \frac{\hat{F}_{SR}K_{SE}}{K_{SE} + K_{LT}} + \frac{\Delta\theta_{VR}K_{SE}K_{LT}}{K_{SE} + K_{LT}} + \hat{B}_{ANT}\Delta\dot{\theta}_{VR_LT_SR} \quad (32)$$

$$T_{VR_SR} = K_{SE}(\Delta\theta_{VR} - \Delta\theta_{VR_LT_SR}) \quad (33)$$

$$\text{Where, } \hat{F}_{SR} = \hat{F}_{SR} + K_{LT}\Delta\theta_{VR_LT_SR} + B_{ANT}\Delta\dot{\theta}_{VR_LT_SR}$$

Details of this calculations are essentially the same as of Lateral recuts presented in Appendix A-1 with the values applied in the vertical directions.

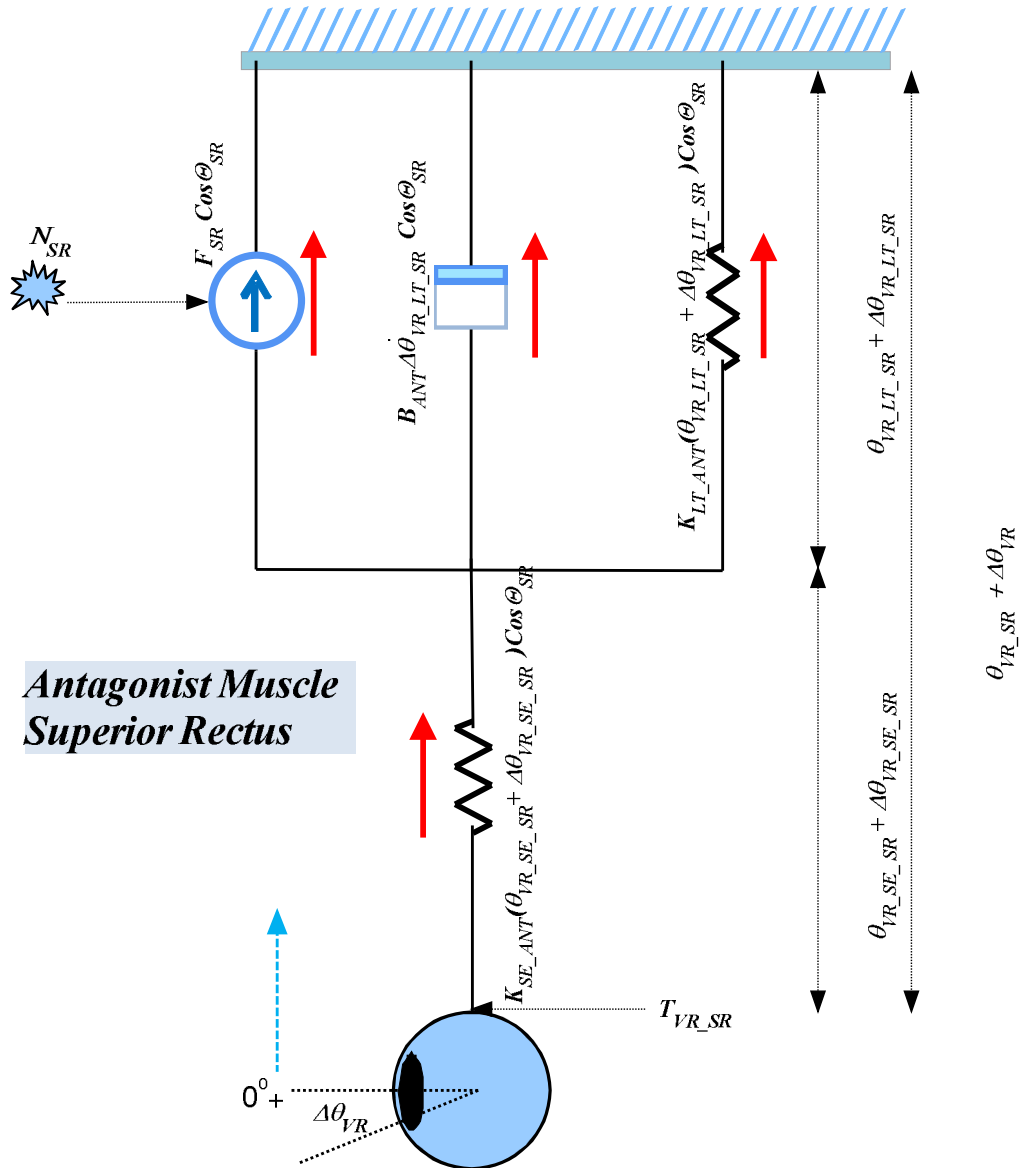


Figure 12. 2DOPMM: Vertical Antagonist Muscle.

Equation of Combined Forces

According to Newton’s second law, the sum of all forces acting on the eye globe equals the acceleration multiplied by the inertia of the eye globe. By applying the law to the horizontal and vertical component of movement:

$$J\Delta\ddot{\theta}_{HR} = T_{HR_MR} - T_{HR_LR} - K_p\Delta\theta_{HR} - B_p\Delta\dot{\theta}_{HR}$$

$$J\Delta\ddot{\theta}_{HR} = -K_{SE}(\Delta\theta_{HR_LT_MR} - \Delta\theta_{HR}) - K_{SE}(\Delta\theta_{HR} - \Delta\theta_{HR_LT_LR}) - K_p\Delta\theta_{HR} \quad (34)$$

$$- B_p\Delta\dot{\theta}_{HR}$$

J - Eye globe's inertia, $\Delta\theta_{HR}$ - horizontal rotation of eye, $\Delta\dot{\theta}_{HR}$ horizontal velocity of the eye rotation, $\Delta\ddot{\theta}_{HR}$ horizontal eye rotation acceleration.

For the vertical component of movement following equation can be written:

$$J\Delta\ddot{\theta}_{VR} = -K_{SE}(\Delta\theta_{VR_LT_IR} - \Delta\theta_{VR}) - K_{SE}(\Delta\theta_{VR} - \Delta\theta_{VR_LT_SR}) - K_p\Delta\theta_{VR} \quad (35)$$

$$- B_p\Delta\dot{\theta}_{VR}$$

The forces represented by equations (34) and (35) are identical for all directions of movement and therefore are not described in latter subsections. Details of the calculations of the following three sections are essentially similar to Left Downward eye movement discussed in previous section and Appendix A, and therefore not provided in detail.

Right Upward eye movement

$$K_{SE}(\Delta\theta_{HR_LT_LR} - \Delta\theta_{HR}) = \frac{\hat{F}_{LR}K_{SE}}{K_{SE} + K_{LT}} - \frac{\Delta\theta_{HR}K_{SE}K_{LT}}{K_{SE} + K_{LT}} - \hat{B}_{AG}\Delta\dot{\theta}_{HR_LT_LR} \quad (36)$$

$$K_{SE}(\Delta\theta_{HR} - \Delta\theta_{HR_LT_MR}) = \frac{\hat{F}_{MR}K_{SE}}{K_{SE} + K_{LT}} + \frac{\Delta\theta_{HR}K_{SE}K_{LT}}{K_{SE} + K_{LT}} + \hat{B}_{ANT}\Delta\dot{\theta}_{HR_LT_MR} \quad (37)$$

$$K_{SE}(\Delta\theta_{VR} - \Delta\theta_{VR_LT_IR}) = \frac{\hat{F}_{IR}K_{SE}}{K_{SE} + K_{LT}} + \frac{\Delta\theta_{VR}K_{SE}K_{LT}}{K_{SE} + K_{LT}} + \hat{B}_{ANT}\Delta\dot{\theta}_{VR_LT_IR} \quad (38)$$

$$K_{SE}(\Delta\theta_{VR_LT_SR} - \Delta\theta_{VR}) = \frac{\hat{F}_{SR}K_{SE}}{K_{SE} + K_{LT}} - \frac{\Delta\theta_{VR}K_{SE}K_{LT}}{K_{SE} + K_{LT}} - \hat{B}_{AG}\Delta\dot{\theta}_{VR_LT_SR} \quad (39)$$

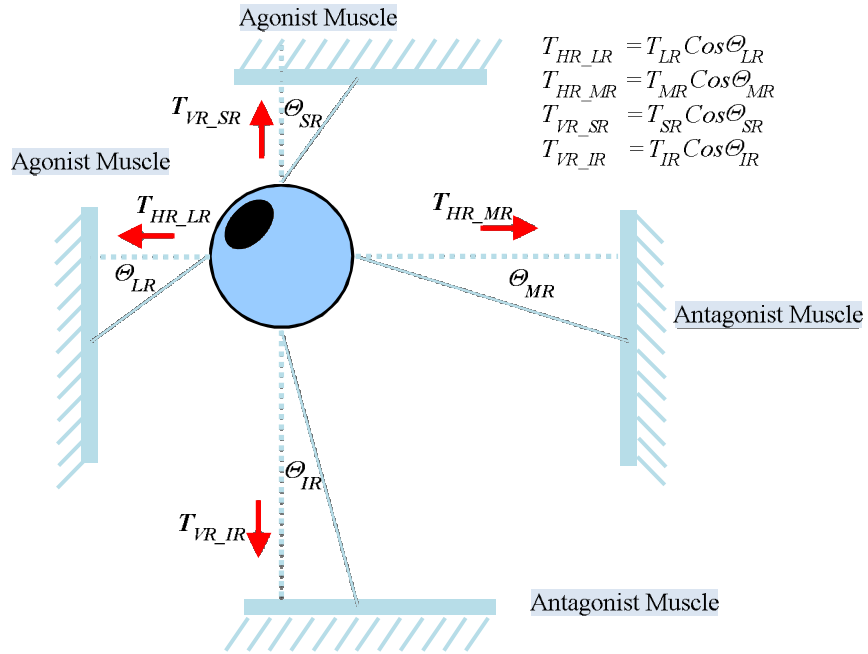


Figure 13. 2DOPMM: Right Upward Rotation.

Left Upward eye movement

$$K_{SE}(\Delta\theta_{VR_LT_SR} - \Delta\theta_{VR}) = \frac{\hat{F}_{SR}K_{SE}}{K_{SE} + K_{LT}} - \frac{\Delta\theta_{VR}K_{SE}K_{LT}}{K_{SE} + K_{LT}} - \hat{B}_{AG}\Delta\dot{\theta}_{VR_LT_SR} \quad (40)$$

$$K_{SE}(\Delta\theta_{HR_LT_MR} - \Delta\theta_{HR}) = \frac{\hat{F}_{MR}K_{SE}}{K_{SE} + K_{LT}} - \frac{\Delta\theta_{HR}K_{SE}K_{LT}}{K_{SE} + K_{LT}} - \hat{B}_{AG}\Delta\dot{\theta}_{HR_LT_MR} \quad (41)$$

$$K_{SE}(\Delta\theta_{VR} - \Delta\theta_{VR_LT_IR}) = \frac{\hat{F}_{IR}K_{SE}}{K_{SE} + K_{LT}} + \frac{\Delta\theta_{VR}K_{SE}K_{LT}}{K_{SE} + K_{LT}} + \hat{B}_{ANT}\Delta\dot{\theta}_{VR_LT_IR} \quad (42)$$

$$K_{SE}(\Delta\theta_{VR} - \Delta\theta_{VR_LT_IR}) = \frac{\hat{F}_{IR}K_{SE}}{K_{SE} + K_{LT}} + \frac{\Delta\theta_{VR}K_{SE}K_{LT}}{K_{SE} + K_{LT}} + \hat{B}_{ANT}\Delta\dot{\theta}_{VR_LT_IR} \quad (43)$$

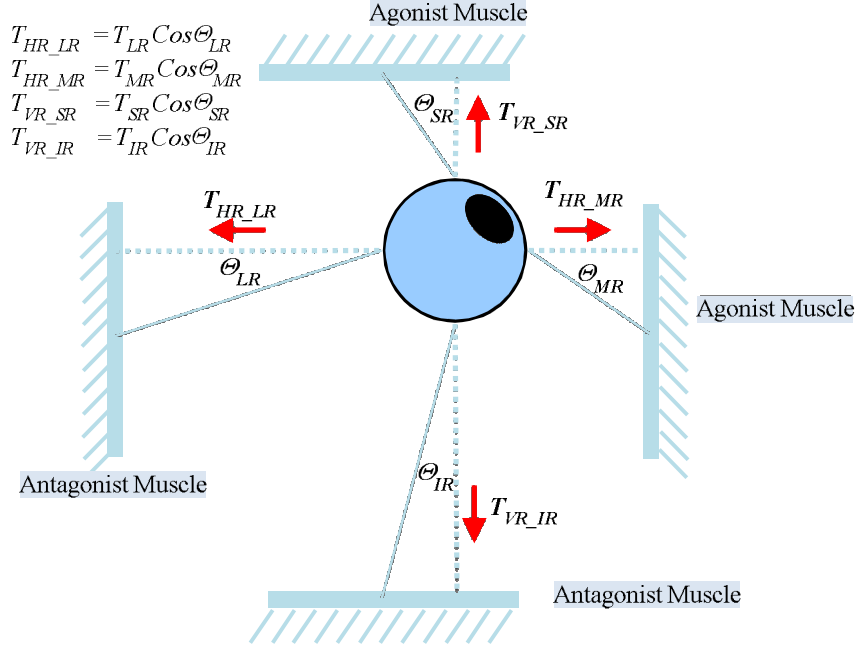


Figure 14. 2DOPMM: Left Upward Rotation.

Right Downward eye movement

$$K_{SE}(\Delta\theta_{HR_LT_LR} - \Delta\theta_{HR}) = \frac{\hat{F}_{LR}K_{SE}}{K_{SE} + K_{LT}} - \frac{\Delta\theta_{HR}K_{SE}K_{LT}}{K_{SE} + K_{LT}} - \hat{B}_{AG}\Delta\dot{\theta}_{HR_LT_LR} \quad (44)$$

$$-K_{SE}(\Delta\theta_{HR} - \Delta\theta_{HR_LT_MR}) \quad (45)$$

$$= -\frac{\hat{F}_{MR}K_{SE}}{K_{SE} + K_{LT}} \pm \frac{\Delta\theta_{HR}K_{SE}K_{LT}}{K_{SE} + K_{LT}} - \hat{B}_{ANT}\Delta\dot{\theta}_{HR_LT_MR}$$

$$K_{SE}(\Delta\theta_{VR_LT_IR} - \Delta\theta_{VR}) = \frac{\hat{F}_{IR}K_{SE}}{K_{SE} + K_{LT}} - \frac{\Delta\theta_{VR}K_{SE}K_{LT}}{K_{SE} + K_{LT}} - \hat{B}_{AG}\Delta\dot{\theta}_{VR_LT_IR} \quad (46)$$

$$K_{SE}(\Delta\theta_{VR} - \Delta\theta_{VR_LT_SR}) = \frac{\hat{F}_{SR}K_{SE}}{K_{SE} + K_{LT}} + \frac{\Delta\theta_{VR}K_{SE}K_{LT}}{K_{SE} + K_{LT}} + \hat{B}_{ANT}\Delta\dot{\theta}_{VR_LT_SR} \quad (47)$$

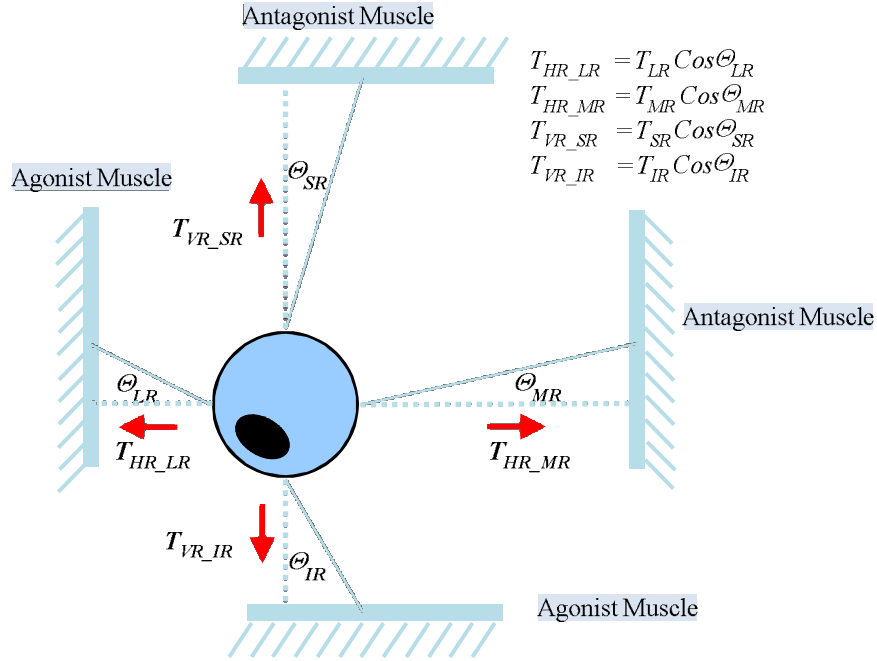


Figure 15. 2DOPMM: Right Downward Rotation.

Examining equations (20)-(47), it is possible to see that in each direction of movement the EOM forces remain in the form of the agonist/antagonist muscle pair presented by the equations (11)-(16).

Simplification of the 2DOPMM Equations

Simplification of the 2DOPMM equations involves dividing all forces acting on the eye globe into strictly the horizontal and vertical components with a set of equations provided for each dimension.

Any translational movement on the 2D plane ($\Delta\theta$) can be separated into the vertical ($\Delta\theta_{VR}$) and horizontal components ($\Delta\theta_{HR}$). This methodology allows simplifying the 2DOPMM into two separate models, where each movement component is simulated by a separate 1D model. Equations (11)-(16) provide the mechanism to achieve this goal.

During upward rotations the vertical component of movement is described by equations (11)-(16) where the superior rectus is the agonist and inferior rectus is the antagonist. During downward movements the roles of the EOMs are switched. During rightward movements the horizontal component of movement will be described by equations (11)-(16) where the lateral rectus is agonist and medial rectus is antagonist. During leftward movements the roles of the EOMs are switched.

Two equations in the matrix form define the 2DOPMM

$$\dot{x} = Ax + u \quad (48)$$

$$\dot{y} = By + c \quad (49)$$

Where A and B are transitional matrixes and u and c are control vectors for the horizontal and vertical components respectively.

Separation into the vertical and horizontal cases provides an opportunity to describe the movement with two sets of equations. This allows solving these equations in parallel in a multi-core enabled system, therefore increasing the speed of computations.

Neuronal Control Signal

The choice of the specific neuronal control signal model during a saccade is an area of active research (Sylvestre & Cullen, 1999). This subsection presents two existing models that were developed for the horizontal saccades, and a new model essentially adhering to the main-sequence relationship. The height of the agonist pulse $N_{AG_sac_pulse}$ provides a significant impact on the properties of the eye movement signal. The impact of the $N_{AG_sac_pulse}$ is ranked 3rd by the Bahill's sensitivity analysis (Bahill, 1980). One of the goals of the 2DOPMM developed in this paper was to find a function that allows

deriving the value of the agonist muscle pulse's height $N_{AG_sac_pulse}$ given the value of the saccade's amplitude θ_{sac_amp} with resulting main-sequence saccade properties close to physiological values of normal humans.

Main-sequence properties are defined by the following formula:

$$\dot{\theta}_{peak} = \dot{\theta}_{MAX} \cdot (1 - e^{-\theta_{sac_amp}/C}) \quad (50)$$

where $\dot{\theta}_{peak}$ is the peak eye velocity recorded during a saccade, $\dot{\theta}_{MAX}$ is the asymptotic peak velocity (500°/s in our study), C is the constant, with value of 14 for normal humans (Leigh & Zee, 2006).

Model I

The $N_{AG_sac_pulse}$ function for the Model I was taken from Bahill's oculomotor plant model (Bahill, 1980).

$$N_{AG_sac_pulse}(\theta_{sac_amp}) = \begin{cases} 55 + 11|\theta_{sac_amp}| \text{ g}, & \text{if } \theta_{sac_amp} \leq 11^\circ \\ 160 + 2|\theta_{sac_amp}| \text{ g}, & \text{if } \theta_{sac_amp} > 11^\circ \end{cases} \quad (51)$$

Where θ_{sac_amp} is saccade's amplitude. The neuronal control signal values are measured in grams (g). They can be converted into the units of spikes/s. The conversion between these two units is done by a constant with a value of 0.48g per spike.

Model II

The parameters of the Model II were taken from the work of Komogortsev and Khan (O. V. Komogortsev & J. Khan, 2009).

$$N_{AG_sac_pulse}(\theta_{sac_onset}, \theta_{sac_amp}) = N_{AG_fix}(|\theta_{sac_onset} + \theta_{sac_amp}|) + \quad (52)$$

$$190 \left(1 - e^{-\frac{|\theta_{sac_amp}|}{50}} \right) g$$

Main assumption of this model is that the brain adds an increase in the neuronal firing frequency, to the step part of the signal, i.e., the pulse signal is not computed from scratch. The magnitude of the increase depends on the amplitude of the saccade. Equation (52) allows separating firing frequency into two components: first component depends on the saccade's onset value and the second component depends on saccade's amplitude. Therefore, if the saccade's amplitude θ_{sac_amp} is zero $N_{AG_sac_pulse}$ would be equivalent to $N_{AG_fix}(|\theta_{sac_onset}|)$. Constants inside of the equation (52) were selected empirically to minimize the error between the model output and the physiological data for large amplitude saccades.

Model III

The goal of the Model III is to minimize the difference between the resulting $\dot{\theta}_{peak}$ value and the $\dot{\theta}_{peak}$ value expressed by normal humans. An error minimization routine was employed using the *lsqnonlin* solver for nonlinear least-squares data fitting problems applying the neuronal pulse height as the parameter for peak velocity error minimization per amplitude. Saccadic amplitudes were selected based on the main-sequence relationship in the range of 1-30° to derive the relationship between the height of the neuronal pulse and the amplitude of the saccade.

The resultant relationship between the saccade amplitude and the $N_{AG_sac_pulse}$ is given by,

$$N_{AG_sac_pulse} = \left(-274.7 \times |\theta_{sac_amp}|^{-0.4269} \right) + 176.9 \quad (53)$$

Model IV

According to (Sylvestre & Cullen, 1999), commonly utilized first-order description of abducens neuron firing rate in (54) provided an adequate model of neuronal activity during saccades, smooth pursuit, and slow phase vestibular nystagmus.

$$FR = b + kE + r\dot{E} \quad (54)$$

Where FR is the firing rate, E and \dot{E} are eye position and velocity, respectively, and b , k , r are constants. The parameters of the Model IV were taken from (Sylvestre & Cullen, 1999), where Bias \bar{b} , Position \bar{k} and Velocity \bar{r} reported as 156, 4.2, and 4.2 respectively. Inside the 2DOPMM, the FR value (neuronal pulse) calculated by the input saccade trajectory from the subject records.

Model V

(Sylvestre & Cullen, 1999) reported that the use of a second-order model, which included an exponentially decaying term or “slide” in notably improved the ability to describe neuronal activity when the eye was moving and also enabled to model abducens neuron discharges during the post-saccadic interval.

$$FR_{NET} = b + kE + r\dot{E} + u\ddot{E} - c\dot{FR} \quad (55)$$

Where FR_{NET} represents the difference between the firing rates of the agonist and antagonist motoneurons, b is the motoneuron’s activity when the eye is stationary in the center of the orbit, E , \dot{E} , and \ddot{E} are eye position, eye velocity, and eye acceleration. \dot{FR} is the derivative of the net firing rate, and the parameters b , k , r , u and c are constants reported as 172, 3.7, 0.42, 0.0077, and 0.015 respectively. During saccades, the net neural

drive FR_{NET} to the extraocular muscles is provided almost entirely by the agonist motoneuron pool, because most antagonist motoneurons cease firing or “pause” during saccadic eye movements.

Remaining Oculomotor Plant Model Parameters

General

Series elasticity coefficient $K_{SE} = 1.9 \text{ g/}^\circ$, length tension coefficient $K_{LT} = 1.9 \text{ g/}^\circ$, damping component coefficient for the viscosity of the eye-orbit and surrounding tissues, combined passive elasticity coefficient of the eye-orbit, both muscles and surrounding tissues $K_p = 0.3 \text{ g/}^\circ$, damping component coefficient for the viscosity of the eye-orbit and surrounding tissue $B_p = 0.06 \text{ g} - \text{sec/}^\circ$, damping coefficients for the agonist and the antagonist $B_{AG} = 0.046 \text{ g} - \text{sec/}^\circ$, $B_{ANT} = 0.022 \text{ g} - \text{sec/}^\circ$, rotational inertial of the eye globe $J = 0.000043 \text{ g} - \text{sec}^2/\text{f}$.

Fixation Related

Neuronal control signal during fixations is

$$N_{AG_fix}(\theta) = (20.72 + 2.38|\theta|) \text{ g}$$

$$N_{ANT_fix}(\theta) = (20.72 - 0.46|\theta|) \text{ g}$$

where $\Delta\theta$ is the angular position of the eye (O. V. Komogortsev & J. Khan, 2009).

Saccade Related

Saccade duration is $t_{sac_offset} - t_{sac_onset} = (2.2 * |\theta_{sac_amp}| + 21) ms.$ (Carpenter, 1977), the onset time of the agonist (antagonist) muscle's pulse after the onset of a saccade is $t_{AG_sac_pulse_onset} - t_{sac_onset} = 3 ms.$, ($t_{ANT_sac_pulse_onset} - t_{sac_onset} = 1 ms.$), the height of the antagonist pulse is $N_{ANT_sac_pulse} = 0.5 g$, the activation/deactivation constants are

$$\tau_{AG_sac_act} = \begin{cases} 11.7 - 0.2 |\theta_{sac_amp}|, & \text{for } |\theta_{sac_amp}| \leq 50 \\ 13 - 0.1 |\theta_{sac_amp}|, & \text{for } |\theta_{sac_amp}| > 50 \end{cases}$$

$$\tau_{AG_sac_de} = 2, \quad \tau_{ANT_sac_ac} = 2.4, \quad \tau_{ANT_sac_de} = 1.9.$$

CHAPTER III

METHODOLOGY

The goal of the 2DOPMM presented in this study is to simulate eye positional signal on a two dimensional plane with characteristics resembling the physiological properties of normal humans. This section presents the description of the experimental setup and metrics that allow verifying the quality of the proposed model.

Apparatus

Eye movement data recording procedures were conducted with Tobii x120 eye tracker (Tobii, 2009), and EyeLink II eye tracker (EyeLink, 2010).

Tobii x120, which is represented by a standalone unit connected to a 19 inch flat panel screen with resolution of 1280x1024. The eye tracker performs binocular tracking with the following characteristics: accuracy 0.5° , spatial resolution 0.2° , drift 0.3° , and eye position sampling frequency of 120Hz. The Tobii x120 model is non-invasive and allows for 300x220x300mm freedom of head movement. Nevertheless, a chin rest was employed for higher accuracy and stability. Subjects were seated approximately 710mm from the screen.

The core of the EyeLink II eye tracker consists of a custom designed high-speed camera connected to a dedicated Host computer. Running on a real-time operating

system, the Host software provides extremely fast eye sample access with incredibly low inter-sample variability, accessed via a set of programming interfaces for multiple operating systems and programming languages. The eye tracker performs binocular tracking with the following characteristics: accuracy 0.5°, spatial resolution 0.05RMS, drift 0.3°, and eye position sampling frequency of 1000Hz. The EyeLink II allows for 220x180x200mm freedom of head movement.

Saccade Invocation Task

Step stimulus was presented to the subjects in a form of a sequence of “jumping” points. Figure 16. 2DOPMM: Saccade Invocation Task.

provides an illustration of the presented sequence and its characteristics. The sequence consisted of total of 14 points invoking 13 stimuli saccades.

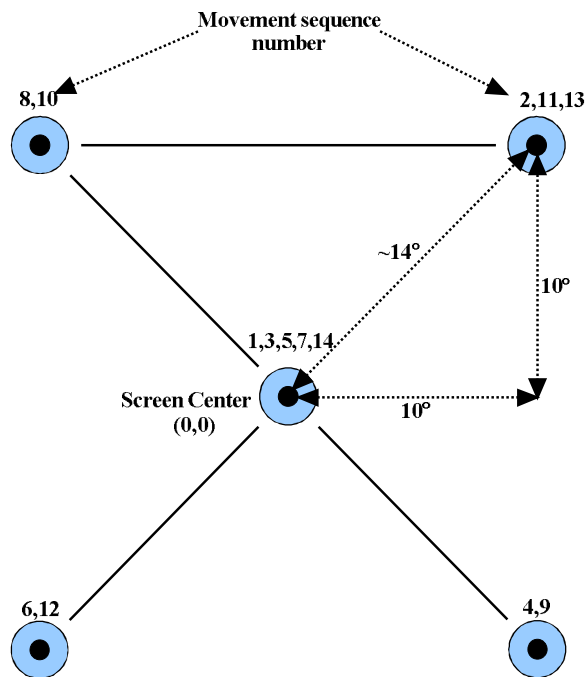


Figure 16. 2DOPMM: Saccade Invocation Task.

After each subsequent jump the point remained stationary for 1.5s before the next jump. The size of the point was approximately 1° of the visual angle with center marked as a black dot. The point was presented with white color, with peripheral background colored in black.

Participants & Quality of the Recorded Data

A total of 68 participants (24 males/ 44 females), 18 – 25 (mean 21.2) years old from the Texas State University-San Marcos campus volunteered for the evaluation test with the Tobii x120 recording session. All participants had normal or corrected-to-normal vision. An eye tracker accuracy tests described in (Koh, Gowda, & Komogortsev, 2009) was conducted prior to each recording. Data recordings from subjects with the average calibration error of more than 3° and valid data percentage of less than 80% were discarded. Only 47 participant records passed these criteria resulting in the average calibration error of $1.21^\circ \pm 0.49$ and valid data percentage of $96.12\% \pm 3.89$.

A total of 27 participants (20 males/ 7 females), 18 – 25 (mean 25.0) years old from the Texas State campus volunteered for the evaluation test with the EyeLink II eye tracker recording session. All participants had normal or corrected-to-normal vision. An eye tracker accuracy tests described in (Koh, et al., 2009) was conducted prior to each recording. Data recordings from subjects with the average calibration error of more than 3° and valid data percentage of less than 80% were discarded. Only 22 participant records passed these criteria resulting in the average calibration error of $1.24^\circ \pm 0.46$.

Saccade data were extracted using Velocity Threshold Identification (I-VT) model, with velocity threshold selected to provide the Saccade Quantitative Score (SQnS) closest to the 100% mark (such SQnS indicates that the amount of detected saccadic behavior equals the amount of saccadic behavior present in the stimulus (O. V. Komogortsev, Jayarathna, Koh, & Gowda, 2010)). Resulting velocity threshold that satisfied this criteria for the Tobii recordings (2D MAIN) was 60°/s with corresponding SQnS of 94.56%. This selection resulted in 2019 saccades with average amplitude of 5.74°±2.82. Resulting velocity threshold that satisfied this criteria for the EyeLink II recordings (2D HIFI) was 130°/s, resulted in 4228 saccades with average amplitude of 6.64°±2.29.

Auxiliary Data Set - DOVES

It is important to verify the performance of the 2DOPMM using different test setups, including eye tracker's accuracy and sampling frequency. The 2D DOVES database was employed for these purposes (Linde, Rajashekhar, Bovik, & Cormack, 2009). The 2D DOVES consists of eye positional recordings collected from 29 human observers as they viewed 101 natural calibrated images. Recordings were done using a high precision dual-Purkinje eye tracker with accuracy of <10 min of arc, precision of about 1 min of arc, a response time of <1 ms, and sampling frequency of 200Hz. We have applied the I-VT classification model with velocity threshold of 60°/s resulted in 300 saccades with average amplitude of 2.51°±0.65.

Sensitivity Analysis and Model Validation

Sensitivity analysis determines the sensitivity of a model to changes in the parameter values (Breierova & Choudhari, 1996). The 2DOPMM sensitivity analysis was performed by simulating a diagonal 20° saccade and comparing it with the perturbed saccades by changing one parameter at a time. +5% change was employed in our tests. The difference between the nominal and perturbed saccades (Δy) was calculated for each millisecond of saccadic duration and was divided by the change in the parameter value ($\Delta\beta$). The resulting ratio was multiplied by the nominal parameter value (β_0). Resulting sensitivity function

$$\Omega(t) = \frac{(\Delta y(t) \times \beta_0)}{\Delta\beta(t)} \quad (56)$$

Above sensitive function represents the sensitivity of β_0 parameter.

The Root Mean Squared Error (RMSE) computed by the equation (57) was employed to indicate a magnitude of error between the simulated and actual signal.

$$RMSE_{2D} = \sqrt{\frac{\sum_{k=1}^n ((\hat{x}_k - x_k)^2 + (\hat{y}_k - y_k)^2)}{n}} \quad (57)$$

Where (x_k, y_k) are the eye position coordinates reported by the eye tracker, and (\hat{x}_k, \hat{y}_k) are the coordinates generated by the 2DOPMM. n represents number of points sampled during a saccade. The $RMSE_{2D}$ is reported in degrees.

Regression analysis, in its simplest form, involves finding the best relationship to explain how the variation in the prediction (or dependent) variable, depends on the variation in the predictor variable (or recorded). The amount of variation in the prediction

variable that is accounted by variation in the recorded variable is measured by the value of the coefficient of determination, often called R^2 adjusted. The closer the R^2 is to 1 the better, because if R^2 adjusted is 1 then the regression model is accounting for all the variation in the prediction variable. By “better” we mean a greater ability to predict the saccadic trajectory. In brief, R^2 is the relative predictive power of the 2DOPMM with its descriptive measure between 0 and 1 defined by,

$$R_{adj}^2 \equiv 1 - \frac{SS_{error}}{SS_{total}}$$

$SS_{err} = \sum_{k=i}^j (x_k - \hat{x}_k)^2$, the sum of squared error or the residual sum of squares

$SS_{tot} = \sum_{k=i}^j (x_k - \bar{x})^2$, the total sum of squares

R^2 statistic was employed to indicate the goodness of fit for horizontal and vertical components of movement (Chatterjee & Hadi, 1986).

CHAPTER IV

RESULTS

Sensitivity Analysis

Table 2 presents the model's parameters which are ranked based on the maximum value of the sensitivity function presented in Methodology. The 2DOPMM results are compared to the Bahill's model (Bahill, 1980). Series elasticity and length tension coefficient K_{SE} and K_{LT} are separated into the agonist (K_{AG_SE} , K_{ANT_SE}) and the antagonist (K_{AG_LT} , K_{ANT_LT}) counterparts to provide more detailed analysis. The PW is the width of the agonist pulse $t_{AG_sac_pulse_offset} - t_{AG_sac_pulse_onset}$. The values of the N_{AG_step} , N_{ANT_step} are mathematically computed from the eye position signal prior and after the saccade and therefore not varied. In case of the Bahill's model initial values of N_{AG_step} , N_{ANT_step} were fixed to constant values.

The resulting order of the model's parameters is similar to the Bahill's model, but not identical. Not surprisingly, the values of the neuronal control signal provides the highest impact on the resulting positional signal. The ranking order of these parameters is important in the OPMM-based biometrics systems (O. V. Komogortsev, Jayarathna, Aragon, et al., 2010).

Table 2. Sensitivity Rankings		
Parameter	Rank Order	
	2DOPMM	Bahill et al. (Bahill, 1980)
$N_{AG_sac_pulse}$	1	3
PW	2	2
K_{AG_SE}	3	5
B_P	4	6
B_{AG}	5	8
$\tau_{AG_sac_ac}$	6	9
K_{AG_LT}	7	4
K_P	8	11
B_{ANT}	9	12
$\tau_{AG_sac_de}$	10	18
K_{ANT_SE}	11	10
K_{ANT_LT}	12	13
J	13	15
$\tau_{ANT_sac_ac}$	14	16
$\tau_{ANT_sac_de}$	15	14
$N_{ANT_sac_pulse}$	16	17
N_{AG_step}	N/A	1
N_{ANT_step}	N/A	7

Model Validation Metrics

Table 3 presents the results of $RMSE_{HR}$ and $RMSE_{VR}$ where records received with x120 eye tracker recorded eye movements are marked as “2D MAIN”. The auxiliary database is marked as “2D DOVES”. The set of the eye movement records received by EyeLink II eye tracker is marked as “2D HIFI”. Bold highlight indicates lower RMSE for the corresponding component of movement. Statistical Significant test presents the resultant F value and p value for the difference between $RMSE_{HR}$ and $RMSE_{VR}$.

Statistical Analysis $RMSE_{HR}$ and $RMSE_{VR}$: The difference in terms of the RMSE between the horizontal component and vertical component was non-significant for all the models (Table 3, RMSE Statistical significance). According to the resultant RMSE, it is evident that the vertical trajectory simulation was more accurate both in 2D Main and 2D

DOVES databases. Furthermore, except for the Model II, the 2D HIFI database was more accurate on horizontal trajectory simulations.

Table 3. Neuronal Control Models, $RMSE_{HR}$ and $RMSE_{VR}$						
RMSE Mean and Standard Deviation						
Model	Saccade	$RMSE_{HR}$		$RMSE_{VR}$		RMSE Statistical Significance
		μ	σ	μ	σ	
I	2D MAIN	0.0463°	0.0293°	0.0451°	0.0304°	(F(1,92)=0.040, p>0.05)
	2D DOVES	0.1607°	0.2693°	0.0746°	0.0856°	(F(1,50)=2.410, p>0.05)
	2D HIFI	1.1387°	0.4384°	1.1454°	0.2972°	F(1,44)=0.004, p>0.05)
II	2D MAIN	0.0473°	0.0305°	0.0455°	0.0308°	(F(1,92)=0.079, p>0.05)
	2D DOVES	0.1492°	0.2121°	0.0708°	0.0679°	(F(1,50)=3.218, p>0.05)
	2D HIFI	1.2733 °	0.4808°	1.1977°	0.0371°	F(1,44)=0.356, p>0.05)
III	2D MAIN	0.0477°	0.0299°	0.0458°	0.0314°	(F(1,92)=0.095, p>0.05)
	2D DOVES	0.1538°	0.2348°	0.0785°	0.1039°	(F(1,50)=2.240, p>0.05)
	2D HIFI	1.0030 °	0.3909°	1.1348°	0.3450°	F(1,44)=1.469, p>0.05)
IV	2D MAIN	0.0470°	0.0299°	0.0459°	0.0310°	(F(1,92)=0.027, p>0.05)
	2D DOVES	0.1521°	0.2257°	0.0797°	0.1098°	(F(1,50)=2.163, p>0.05)
	2D HIFI	1.1207°	0.4162°	1.1919°	0.3072°	F(1,44)=0.435, p>0.05)
V	2D MAIN	0.0469°	0.0296°	0.0459°	0.0310°	(F(1,92)=0.024, p>0.05)
	2D DOVES	0.1560°	0.2447°	0.0816°	0.1189°	(F(1,50)=2.194, p>0.05)
	2D HIFI	1.1773°	0.4294°	1.2601°	0.3183°	F(1,44)=0.551, p>0.05)

Statistical Analysis $RMSE_{HR}$: The difference in terms of the RMSE between the neuronal control models was non-significant for 2D MAIN (F(4,230)=0.015, p>0.05). Same was true for the 2D Doves (F(4,125)=0.009, p>0.05), and 2D HIFI (F(4,110)=1.178, p>0.05).

Statistical Analysis $RMSE_{VR}$: The difference in terms of the RMSE between the neuronal control models was non-significant for 2D MAIN (F(4,230)=0.006, p>0.05), Same was true for the 2D Doves (F(4,125)=0.049, p>0.05), and 2D HIFI (F(4,110)=0.527, p>0.05).

Statistical Analysis R^2_{HR} : The difference in terms of the R^2 between the neuronal control models was non-significant for 2D MAIN (F(4,230)=0.000, p>0.05), Same was true for the 2D Doves (F(4,125)=0.000, p>0.05), and 2D HIFI (F(4,110)=0.155, p>0.05).

Statistical Analysis R^2_{VR} : The difference in terms of the R^2 between the neuronal control models was non-significant for 2D MAIN ($F(4,230)=0.000$, $p>0.05$), Same was true for the 2D Doves ($F(4,125)=0.000$, $p>0.05$), and 2D HIFI ($F(4,110)=0.155$, $p>0.05$).

Table 4 presents the results of $RMSE_{HR}$ and $RMSE_{VR}$ where records received with x120 eye tracker recorded eye movements are marked as “2D MAIN”. The auxiliary database is marked as “2D DOVES”. The set of the eye movement records received by EyeLink II eye tracker is marked as “2D HIFI”. Bold highlight indicates higher R^2 for the corresponding component of movement. Statistical Significant test presents the resultant F value and p value for the difference between R^2_{HR} and R^2_{VR} . Asterisk highlights statistically significant results.

Table 4. Neuronal Control Models, $RMSE_{2D}$ and R^2						
RMSE and R^2 Mean and Standard Deviation.						
Model	Saccade	$RMSE_{2D}$		R^2		R^2 Statistical Significance
		μ	σ	HR	VR	
I	2D MAIN	0.0668°	0.0386°	0.6889	0.6679	($F(1,92)=1.049$, $p>0.05$)
	2D DOVES	0.1800°	0.2807°	0.6344	0.5794	*($F(1,50)=15.21$, $p<0.05$)
	2D HIFI	1.6227°	0.5051°	0.5748	0.5822	($F(1,44)=0.278$, $p>0.05$)
II	2D MAIN	0.0678°	0.0397°	0.6891	0.6680	($F(1,92)=1.069$, $p>0.05$)
	2D DOVES	0.1679°	0.2205°	0.6346	0.5799	* $F(1,50)=15.55$, $p<0.05$)
	2D HIFI	1.7582°	0.5764°	0.5713	0.5822	($F(1,44)=0.575$, $p>0.05$)
III	2D MAIN	0.0683°	0.0398°	0.6891	0.6680	($F(1,92)=1.061$, $p>0.05$)
	2D DOVES	0.1746°	0.2533°	0.6344	0.5789	* $F(1,50)=15.19$, $p<0.05$)
	2D HIFI	1.5178°	0.4851°	0.5759	0.5813	($F(1,44)=0.145$, $p>0.05$)
IV	2D MAIN	0.0679°	0.0395°	0.6889	0.6679	($F(1,92)=1.054$, $p>0.05$)
	2D DOVES	0.1740°	0.2494°	0.6347	0.5786	* $F(1,50)=15.34$, $p<0.05$)
	2D HIFI	1.6432°	0.4929°	0.5809	0.5864	($F(1,44)=0.153$, $p>0.05$)
V	2D MAIN	0.0678°	0.0393°	0.6889	0.6679	($F(1,92)=1.049$, $p>0.05$)
	2D DOVES	0.1783°	0.2706°	0.6346	0.5784	* $F(1,50)=15.07$, $p<0.05$)
	2D HIFI	1.7308°	0.5130°	0.5814	0.5866	($F(1,44)=0.138$, $p>0.05$)

Statistical Analysis R^2_{HR} and R^2_{VR} : The difference in terms of the R^2 between the horizontal component and vertical component was non-significant for the 2D Main and

2D HIFI database and significant for the 2D DOVES database (Table 4, R^2 Statistical significance). According to the resultant R^2 , it is evident that the horizontal trajectory simulation was more accurate both in 2D Main and 2D Doves for all the models and vertical trajectory simulation was more accurate for the 2D HIFI database.

Statistical Analysis $RMSE_{2D}$ 2D MAIN: The resulting RMSE for the 2D MAIN database for all models was at least 0.5° as small than the computed distance between the left and right eyes (mean $2.01^\circ \pm 0.73$). All neuronal control models yielded high positional accuracy. Model I yielded lowest average $RMSE_{2D}$. Model II and V were the second best, and Model IV, Model III were third, and fourth respectively. The difference in terms of RMSE between the models was statistically non-significant ($F(4,230)=0.009$, $p>0.05$).

Statistical Analysis $RMSE_{2D}$ 2D DOVES: The 2D DOVES database contains an averaged positional signal between both eyes and therefore, the positional accuracy between the two eyes cannot be reported. Model II yielded lowest average $RMSE_{2D}$. Model IV and III were the second best, and Model V, Model I were third, and fourth respectively. The difference in terms of RMSE between the models was statistically non-significant ($F(4,125)=0.009$, $p>0.05$).

Statistical Analysis $RMSE_{2D}$ 2D HIFI: The 2D HIFI database contains only a single eye position signal and therefore, the positional accuracy between the two eyes cannot be reported. Model III yielded lowest average $RMSE_{2D}$. Model II and IV were the second best, and Model V, and Model I were third, and fourth respectively. The difference in terms of RMSE between the models was statistically non-significant ($F(4,110)=0.787$, $p>0.05$).

Statistical Analysis $RMSE_{2D}$ between databases: The RMSE values for each model between the datasets were statistically significant at the .05 alpha levels. Model I, Model II, Model III, Model IV and Model V yielding corresponding results (F (2,93) =245.3, p<0.05), (F (2,93) =259.8, p<0.05), (F (2,93) =237.6, p<0.05), (F (2,93) =276.9, p<0.05), and (F (2,93) =279.9, p<0.05) respectively.

In general, the $RMSE_{2D}$ and the R^2 values showed a trend of lowering accuracy with higher device sampling frequency. Compared to the obtained subject saccade trajectory records, 2D DOVES database consists of least number of saccades per subject pool (300 total saccades), 2D MAIN with second best number of saccades per subject pool (2019 total saccades) and 2D HIFI with highest number of saccades per subject pool (4228 total saccades).

Main Sequence Relationship

Table II indicates that the pulse of the agonist EOM $N_{AG_sac_pulse}$ provides the most significant impact on the properties of the eye movement signal. One of the goals of the 2DOPMM developed in this study was to explore the existing models of the neuronal control signal in terms of the closeness of the output signal to the main sequence relationship of normal humans.

Main sequence properties are defined by the following formula:

$$\dot{\theta}_{peak} = \dot{\theta}_{MAX} \cdot (1 - e^{-\theta_{sac_amp}/C}) \quad (58)$$

where $\dot{\theta}_{peak}$ is the peak eye velocity recorded during a saccade, $\dot{\theta}_{MAX}$ is the asymptotic peak velocity (500°/s in our study), C is the constant, with value of 14 for normal humans (Leigh & Zee, 2006).

To test the neuronal activity impact in terms of the main sequence relationship, the 1DOPMM was innervated by the neuronal control signal provided by Model I, Model II and Model III. Saccades were simulated with horizontal amplitudes of 0-30°. Figure 17 illustrates the results. This proves that in deed the Model III is closely matched with the main sequence relationship and Model I and Model II are yielding values deviating from the main sequence.

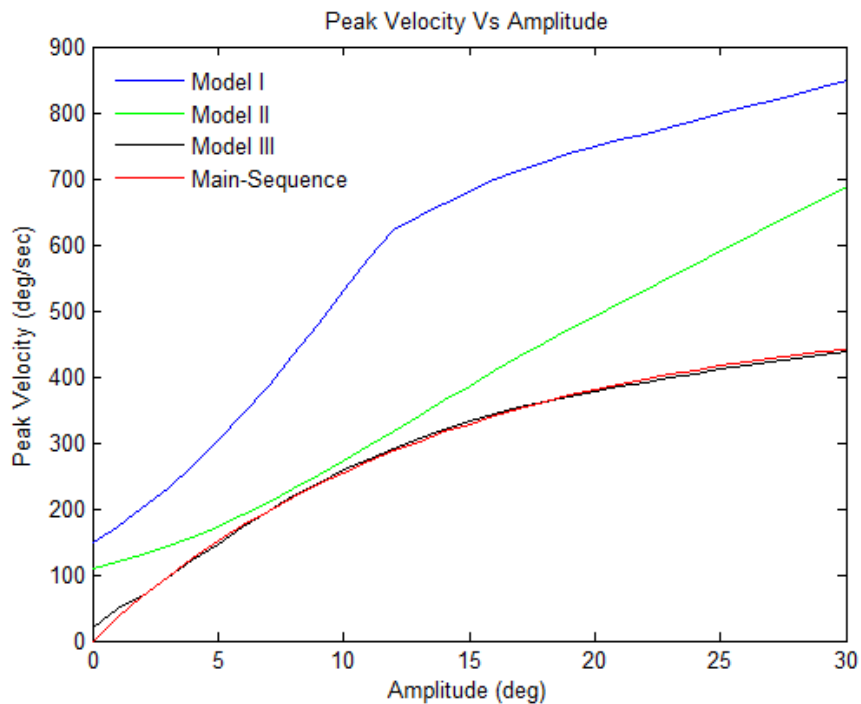


Figure 17. 1DOPMM: Main Sequence Relationship.

For each neuronal control signal model with horizontal stimulus saccades of amplitude 0-30°, with onset (0, 0).

To test the 2DOPMM in terms of the main sequence relationship the model was innervated by the neuronal control signal provided by Model I, Model II and Model III. Saccades were simulated with amplitudes of 0-30° and directed in angles of 0-90°. Figure

18 illustrates the results. The Model I and Model II produced main sequence signatures for what can be classified as “fast” saccades (Leigh & Zee, 2006). The Model I yielded the $R^2=0.95$ and the $RMSE=401^\circ/s$, the Model II yielded lower accuracy error the $RMSE=137^\circ/s$ but lower fit $R^2=0.90$ to the main sequence relationship. The Model III relatively matched with the main sequence relationship with a better accuracy error $RMSE=41^\circ/s$ and a better fit $R^2=0.97$ compared to Model I and Model II. This result indicates the importance of additional research in terms of the neuronal control models for the 2D saccades.

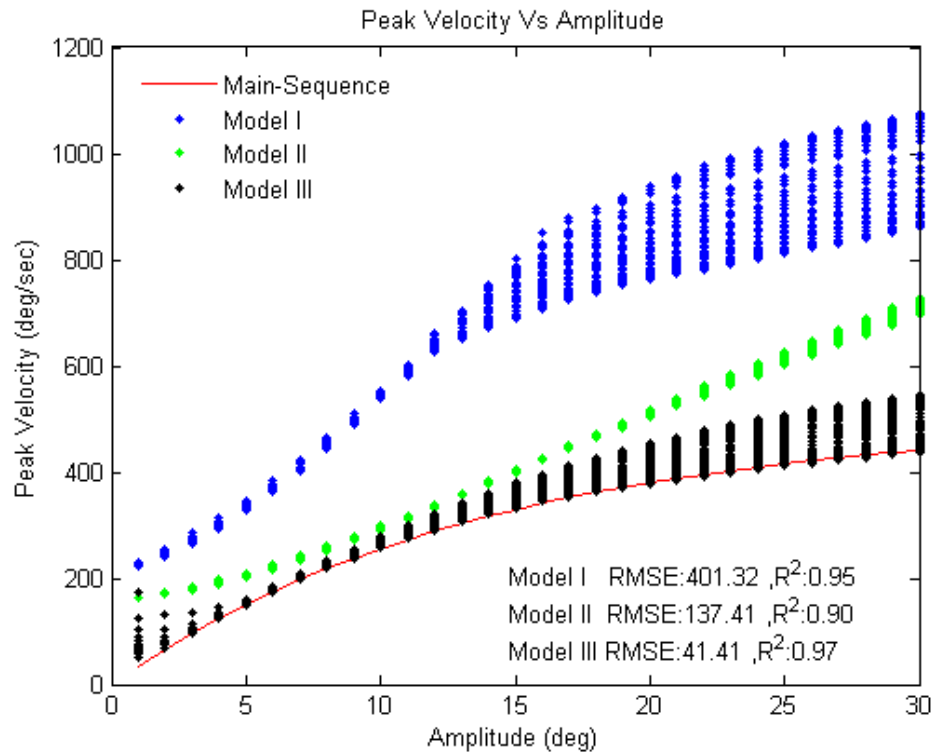


Figure 18. 2DOPMM: Main Sequence Relationship.

For each neuronal control signal model, amplitudes of 0-30° and directed in angles of 0-90°, with onset at (0,0) with 2821 sample points.

Both of the previous figures are the results of model innervations with a fixed onset on the (0,0). In order to verify the outcome of the three models on 1DOPMM and 2DOPMM, the onset/offset was generated randomly and resultant outcome recorded for investigation. Because the amplitude values are different in each situation for each model, the model comparisons with the main-sequence are handled in separate diagrams. The Figure 19 and Figure 20 represent the outcome of the three models. In 2DOPMM the Model III showed a better error RMSE:152°/s compared to Model I RMSE:470°/s and Model II RMSE:172°/s. In terms of better fit, the Model II represents the R^2 : 0.50 and Model I R^2 : 0.58. Even though the Model III fit shows R^2 of 0.26, it can be by hypothesis that this particular result is due to the scattered nature of data points.

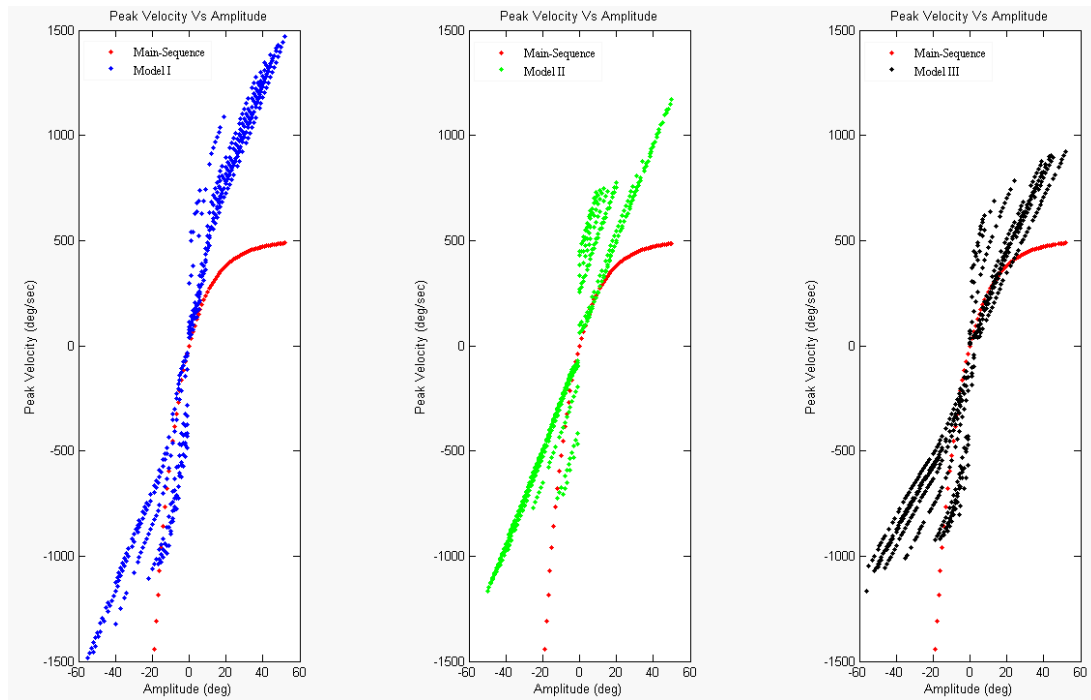


Figure 19. 1DOPMM: Random Onset/Offset Main Sequence Relationship.

For each neuronal control signal model, horizontal amplitudes of 0-30°, with random onset/offset, and 1000 sample points, and both positive and negative saccade amplitudes.

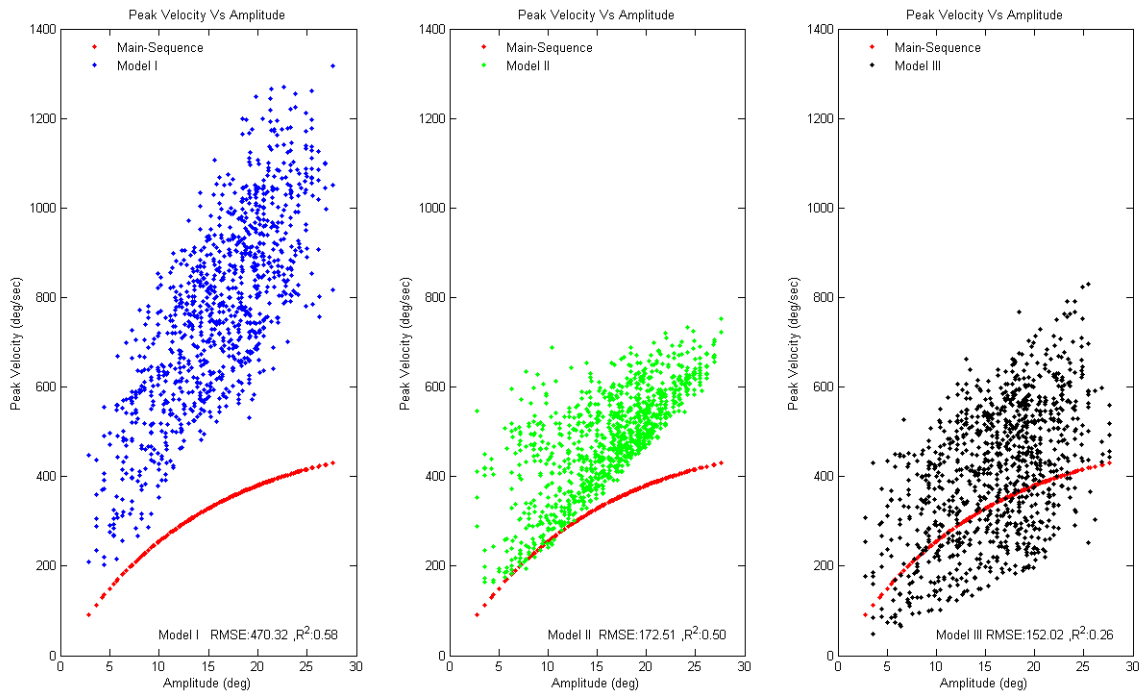


Figure 20. 2DOPMM: Random Onset/Offset Main Sequence Relationship.

For each neuronal control signal model, amplitudes of 0-30° and directed in angles of 0-90°, with random onset, 1000 sample points and only positive saccade amplitudes.

CHAPTER IV

CONCLUSION & FUTURE WORK

Eye mathematical modeling can be used to advance such fast growing areas of research as medicine, human computer interaction, and software usability. In this research study we have created a two dimensional mechanical model of the human eye that is capable of generating eye movement trajectories with both vertical and horizontal components during fast eye movements (saccades) given the coordinates of the onset point, the direction of movement and the value of the saccade amplitude.

The important contribution of the proposed model to the field of bio engineering is the ability to compute individual extraocular muscle forces during a saccade – something that have not been done before to the best of our knowledge.

Our model evolved from a one dimensional version which was successfully employed for eye movement prediction as a tool for delay compensation in Human Computer Interaction with direct eye-gaze input (O. Komogortsev, V. & Khan, 2008), (O. V. Komogortsev & J. I. Khan, 2009) and suggested for the effort estimation for improving the usability of the graphical user interfaces (Tamir, Komogortsev, & Mueller, 2008). Two dimensional version of the model proposed in this paper extends those capabilities to a two dimensional plane.

This research study developed a two dimensional, linear model of the Oculomotor Plant, which is capable of simulating fixation and saccade eye movement signal on a two dimensional plane. The model consists of four extraocular muscles, their properties, and the eye globe's components such as: muscle location, elasticity, viscosity, rotational inertia, muscle active state tension, length tension and force velocity relationships and realistic neuronal control signal properties. The strength of the proposed model is its linear design and the ability to be represented as two separate one dimensional models that perform parallel computation of the horizontal and vertical components of movement. A 1DOPMM model is required to process 36 multiplications (6x6 transition matrix) for a single run, and 2DOPMM is required to process 144 multiplications (12x12 transition matrix) for a similar run. In this regard, a single 2DOPMM requires two times more multiplications than two 1DOPMM models. Such design would allow the model to be applicable to the real-time eye gaze aware systems.

Sensitivity analysis of the model's parameters indicates the most substantial impact of the neuronal control signal properties on the resulting positional signal. The exact property of the neuronal control signal during saccades is an area of active research. Three separate models for generation of the neuronal control were considered in this paper, including two models suggested by - the first model was developed by Bahill (Bahill, 1980), the second by Komogortsev and Khan (O. V. Komogortsev & J. Khan, 2009) and third model specifically developed using the 1DOPMM model to test the performance on 2DOPMM. All three models were originally developed for the horizontal saccades. Model I to IV except model V provided an accurate eye positional signal with positional error 0.5° as small as the difference between both eyes. All five models

provided an acceptable fit to the positional data. The high RMSE for the HIFI data is possibly a result of: 1) lower accuracy of the recordings 2) incorrect threshold selection. Therefore, further study on this is proposed to clarify the trend of having higher RMSE with an eye tracking device of a high sampling frequency. The fit to the main sequence relationship was adequate, but with large velocity errors, indicating the need for the development of the new models of the neuronal control for the non horizontal eye movements. Presented 2DOPMM can be employed as a tool to facilitate this type of research.

In the future the 2DOPMM can be applied to the novel Human Computer Interaction techniques and biometric systems as conducted with 1DOPMM model in (O. V. Komogortsev, et al., 2009) and (O. V. Komogortsev, Jayarathna, Aragon, et al., 2010).

APPENDIX A

A.1 Lateral Rectus

Equations (18), and (19), can be combined to the equation,

$$\begin{aligned}
 -K_{SE}(\theta_{HR_SE_LR} + \Delta\theta_{HR_SE_LR}) + F_{LR} + K_{LT}(\theta_{HR_LT_LR} + \Delta\theta_{HR_LT_LR}) & \quad (59) \\
 + B_{ANT}\Delta\dot{\theta}_{HR_LT_LR} = 0
 \end{aligned}$$

Taking into consideration that

$$\theta_{HR_LR} = \theta_{HR_LT_LR} + \theta_{HR_SE_LR} \text{ and } \Delta\theta_{HR} = \Delta\theta_{HR_LT_LR} + \Delta\theta_{HR_SE_LR}$$

the following equation can be calculated:

$$\theta_{HR_LR} + \Delta\theta_{HR} = \theta_{HR_LT_LR} + \theta_{HR_SE_LR} + \Delta\theta_{HR_LT_LR} + \Delta\theta_{HR_SE_LR}$$

And rearranging the previous equation,

$$\theta_{HR_LR} + \Delta\theta_{HR} - \theta_{HR_LT_LR} - \Delta\theta_{HR_LT_LR} = \theta_{HR_SE_LR} + \Delta\theta_{HR_SE_LR}$$

Inserting above equation into (59)

$$\begin{aligned}
 -K_{SE}(\theta_{HR_LR} + \Delta\theta_{HR} - \theta_{HR_LT_LR} - \Delta\theta_{HR_LT_LR}) + F_{LR} & \quad (60) \\
 + K_{LT}(\theta_{HR_LT_LR} + \Delta\theta_{HR_LT_LR}) + B_{ANT}\Delta\dot{\theta}_{HR_LT_LR} = 0
 \end{aligned}$$

$$\begin{aligned}
 -K_{SE}(\Delta\theta_{HR} - \Delta\theta_{HR_LT_LR}) + F_{LR} - K_{SE}(\theta_{HR_LR} - \theta_{HR_LT_LR}) & \quad (61) \\
 + K_{LT}(\theta_{HR_LT_LR} + \Delta\theta_{HR_LT_LR}) + B_{ANT}\Delta\dot{\theta}_{HR_LT_LR} = 0
 \end{aligned}$$

Assigning, $\hat{F}_{LR} = F_{LR} + K_{SE}\theta_{HR_LT_LR} - K_{SE}\theta_{HR_LR} + K_{LT}\theta_{HR_LT_LR}$

Written as,

$$K_{SE}(\Delta\theta_{HR} - \Delta\theta_{HR_LT_LR}) = \hat{F}_{LR} + K_{LT}\Delta\theta_{HR_LT_LR} + B_{ANT}\Delta\dot{\theta}_{HR_LT_LR} \quad (62)$$

New equation for T_{HR_LR} can be written as,

$$T_{HR_LR} = K_{SE}(\Delta\theta_{HR} - \Delta\theta_{HR_LT_LR}) \quad (63)$$

$$T_{HR_LR} = \hat{F}_{LR} + K_{LT}\Delta\theta_{HR_LT_LR} + B_{ANT}\Delta\dot{\theta}_{HR_LT_LR} \quad (64)$$

Using equation (63), $\Delta\theta_{HR_LT_LR}$ can be calculated as, $\Delta\theta_{HR_LT_LR} = \Delta\theta_{HR} - \frac{T_{HR_LR}}{K_{SE}}$

This result can be substituted into (64) to calculate,

$$T_{HR_LR} = \hat{F}_{LR} + K_{LT}\left(\Delta\theta_{HR} - \frac{T_{HR_LR}}{K_{SE}}\right) + B_{ANT}\Delta\dot{\theta}_{HR_LT_LR} \quad (65)$$

Equation (65) can be transformed into,

$$T_{HR_LR} = \frac{\hat{F}_{LR}K_{SE}}{K_{SE} + K_{LT}} + \Delta\theta_{HR}\frac{K_{SE}K_{LT}}{K_{SE} + K_{LT}} + \frac{B_{ANT}K_{SE}}{K_{SE} + K_{LT}}\Delta\dot{\theta}_{HR_LT_LR} \quad (66)$$

By assigning $\hat{B}_{ANT} = \frac{B_{ANT}K_{SE}}{K_{SE} + K_{LT}}$

$$T_{HR_LR} = \frac{\hat{F}_{LR}K_{SE}}{K_{SE} + K_{LT}} + \frac{\Delta\theta_{HR}K_{SE}K_{LT}}{K_{SE} + K_{LT}} + \hat{B}_{ANT}\Delta\dot{\theta}_{HR_LT_LR} \quad (67)$$

Equations (63) and (67) are the same as equations (18), and (19).

A.2 Medial rectus

Equations (22) and (23), can be combined to the equation,

$$K_{SE}(\theta_{HR_SE_MR} + \Delta\theta_{HR_SE_MR}) - F_{MR} - K_{LT}(\theta_{HR_LT_MR} - \Delta\theta_{HR_LT_MR}) \quad (68)$$

$$+ B_{AG}\Delta\dot{\theta}_{HR_LT_MR} = 0$$

Taking into consideration that $\theta_{HR_MR} = \theta_{HR_LT_MR} + \theta_{HR_SE_MR}$ and $\Delta\theta_{HR} = \Delta\theta_{HR_LT_MR} - \Delta\theta_{HR_SE_MR}$

the following equation can be calculated:

$$\theta_{HR_MR} - \Delta\theta_{HR} = \theta_{HR_LT_MR} + \theta_{HR_SE_MR} - \Delta\theta_{HR_LT_MR} + \Delta\theta_{HR_SE_MR}$$

And rearranging the previous equation,

$$\theta_{HR_MR} - \Delta\theta_{HR} - \theta_{HR_LT_MR} + \Delta\theta_{HR_LT_MR} = \theta_{HR_SE_MR} + \Delta\theta_{HR_SE_MR}$$

Inserting above equation into (68)

$$K_{SE}(\theta_{HR_MR} - \Delta\theta_{HR} - \theta_{HR_LT_MR} + \Delta\theta_{HR_LT_MR}) - F_{MR} \quad (69)$$

$$- K_{LT}(\theta_{HR_LT_MR} - \Delta\theta_{HR_LT_MR}) + B_{AG}\Delta\dot{\theta}_{HR_LT_MR} = 0$$

$$K_{SE}(-\Delta\theta_{HR} + \Delta\theta_{HR_LT_MR}) - F_{MR} + K_{SE}(\theta_{HR_MR} - \theta_{HR_LT_MR}) \quad (70)$$

$$- K_{LT}(\theta_{HR_LT_MR} - \Delta\theta_{HR_LT_MR}) + B_{AG}\Delta\dot{\theta}_{HR_LT_MR} = 0$$

Assigning, $\hat{F}_{MR} = F_{MR} - K_{SE}(\theta_{HR_MR} - \theta_{HR_LT_MR}) + K_{LT}(\theta_{HR_LT_MR})$

Written as,

$$-K_{SE}(\Delta\theta_{HR_LT_MR} - \Delta\theta_{HR}) = -\hat{F}_{MR} + K_{LT}\Delta\theta_{HR_LT_MR} + B_{AG}\Delta\dot{\theta}_{HR_LT_MR} \quad (71)$$

New equation for T_{HR_MR} can be written as,

$$T_{HR_MR} = -K_{SE}(\Delta\theta_{HR_LT_MR} - \Delta\theta_{HR}) \quad (72)$$

$$T_{HR_MR} = -\hat{F}_{MR} + K_{LT}\Delta\theta_{HR_LT_MR} + B_{AG}\Delta\dot{\theta}_{HR_LT_MR} \quad (73)$$

Using equation (72), $\Delta\theta_{HR_LT_MR}$ can be calculated as, $\Delta\theta_{HR_LT_MR} = \Delta\theta_{HR} - \frac{T_{HR_MR}}{K_{SE}}$

This result can be substituted into (73) to calculate,

$$T_{HR_MR} = -\hat{F}_{MR} + K_{LT}\left(\Delta\theta_{HR} - \frac{T_{HR_MR}}{K_{SE}}\right) + B_{AG}\Delta\dot{\theta}_{HR_LT_MR} \quad (74)$$

Equation (74) can be transformed into,

$$T_{HR_MR} = -\frac{\hat{F}_{MR}K_{SE}}{K_{SE} + K_{LT}} + \Delta\theta_{HR}\frac{K_{SE}K_{LT}}{K_{SE} + K_{LT}} + \frac{B_{AG}K_{SE}}{K_{SE} + K_{LT}}\Delta\dot{\theta}_{HR_LT_MR} \quad (75)$$

By assigning $\hat{B}_{AG} = \frac{B_{AG}K_{SE}}{K_{SE}+K_{LT}}$

$$T_{HR_MR} = -\frac{\hat{F}_{MR}K_{SE}}{K_{SE} + K_{LT}} + \frac{\Delta\theta_{HR}K_{SE}K_{LT}}{K_{SE} + K_{LT}} + \hat{B}_{AG}\Delta\dot{\theta}_{HR_LT_MR} \quad (76)$$

Equations (75) and (76) are the same as equations (24) and (25).

REFERENCES

- Bahill, A. T. (1980). Development, validation and sensitivity analyses of human eye movement models. *CRC Critical Reviews in Bioengineering*, 4, 311-355.
- Breierova, L., & Choudhari, M. (1996). An Introduction to Sensitivity Analysis. Retrieved from <http://sysdyn.clexchange.org/sdep/Roadmaps/RM8/D-4526-2.pdf>
- Carpenter, R. H. S. (1977). *Movements of the Eyes*. London: Pion.
- Chatterjee, S., & Hadi, A. S. (1986). Influential Observations, High Leverage Points, and Outliers in Linear Regression. *Statistical Science*, 1, 379–416.
- Clark, M. R., & Stark, L. (1974). Control of human eye movements. *Mathematical Bioscience*, 20, 91-265.
- Crawford, J. D., Martinez-Trujillo, J. C., & Klier, E. M. (2003). Neural control of three-dimensional eye and head movements. *Current Opinion in Neurobiology*, 13(6), 655-662.
- EyeLink. (2010). EyeLink 1000: SR Research.
- Koh, D. H., Gowda, S. A. M., & Komogortsev, O. V. (2009). *Input evaluation of an eye-gaze-guided interface: kalman filter vs. velocity threshold eye movement identification*. Paper presented at the Proceedings of the 1st ACM SIGCHI symposium on Engineering interactive computing systems.
- Komogortsev, O., V., & Khan, J. (2008). *Eye Movement Prediction by Kalman Filter with Integrated Linear Horizontal Oculomotor Plant Mechanical Model*. Paper presented at the ETRA Symposium 2008, Savannah, GA.
- Komogortsev, O. V. (2007). *Eye Movement Prediction by Oculomotor Plant Modeling with Kalman Filter*. Unpublished Dissertation, Kent State University, Kent, OH USA

- Komogortsev, O. V., & Jayarathna, U. K. S. (2008, October 8-10). *2D Oculomotor Plant Mathematical Model for eye movement simulation*. Paper presented at the 8th IEEE International Conference on BioInformatics and BioEngineering (BIBE).
- Komogortsev, O. V., Jayarathna, U. K. S., Aragon, C. R., & Mechehoul, M. (2010). *Biometric Identification via an Oculomotor Plant Mathematical Model*. Paper presented at the Eye Tracking Research & Applications (ETRA'2010), Austin, TX.
- Komogortsev, O. V., Jayarathna, U. K. S., Koh, D. H., & Gowda, M. (2010, March 22-24). *Qualitative and Quantitative Scoring and Evaluation of the Eye Movement Classification Algorithms*. Paper presented at the ACM Eye Tracking Research & Applications Symposium, Austin, TX.
- Komogortsev, O. V., & Khan, J. (2009). Eye Movement Prediction by Oculomotor Plant Kalman Filter with Brainstem Control. *Journal of Control Theory and Applications*, 7(1), 14-22.
- Komogortsev, O. V., & Khan, J. I. (2009). Eye Movement Prediction by Oculomotor Plant Kalman Filter with Brainstem Control. *Journal of Control Theory and Applications*, 7(1).
- Komogortsev, O. V., Ryu, Y. S., Do, H. K., & Gowda, S. A. M. (2009, October 29-31). *Instantaneous Saccade Driven Eye Gaze Interaction*. Paper presented at the ACM International Conference on Advances in Computer Entertainment Technology.
- Leigh, R. J., & Zee, D. S. (2006). *The Neurology of Eye Movements*: Oxford University Press.
- Linde, I. V. D., Rajashekhar, U., Bovik, A. C., & Cormack, L. K. (2009). DOVES: A database of visual eye movements. *Spatial Vision*, 22(2), 161-177.
- Lockwood-Cooke, P., Martin, C. F., & Schovanec, L. (1999). *A dynamic 3-D model of ocular motion*. Paper presented at the IEEE Conference on Decision and Control.
- Martin, C. F., & Schovanec, L. (1998). Muscle Mechanics and Dynamics of Ocular Motion. *Journal of Mathematical Systems, Estimation, and Control*, 8(2), 233-236.

- Polpitiya, A. D., Ghosh, B. K., Martin, C. F., & Schovanec, L. (2002). *Modeling and Control of 3D Eye Movement with Musculotendon Dynamics*. Paper presented at the 2002 IFAC World Congress,, Barcelona.
- Raphan, T. (1998). Modeling Control of Eye Orientation in Three Dimensions. I. Role of Muscle Pulleys in Determining Saccadic Trajectory. *J Neurophysiol*, 79(5), 2653-2667.
- Robinson, D. A. (1973). Models of the saccadic eye movement control system. *Kybernetic*, 14(2), 71-83.
- Sparks, D. L. (2002). The brainstem control of saccadic eye movements. *Nat. Rev. Neurosci.*, 3(12), 952-964.
- Sylvestre, P. A., & Cullen, K. E. (1999). Quantitative Analysis of Abducens Neuron Discharge Dynamics During Saccadic and Slow Eye Movements. *Neurophysiology* 82 (5), 2612-2632.
- Tamir, D., Komogortsev, O., & Mueller, C. (2008). *An Effort and Time Based Measure of Usability*. Paper presented at the 30th International Conference on Software Engineering.
- Tobii. (2009). Tobii technology. from <http://www.tobii.com>
- Tweed, D. (1997). Three-Dimensional Model of the Human Eye-Head Saccadic System. *The Journal of Neurophysiology*, 77(2), pp. 654-666.
- Westheimer, G. (1954). Mechanism of saccadic eye movements. *A.M.A. Archives of Ophthalmology*, 52, 710-724.
- Wilkie, D. R. (1976). Muscle. *Studies in Biology*, 11.

VITA

Sampath Jayarathna was born and raised in Kurunegala, Sri Lanka and matriculated at St. Anne's College, Sri Lanka. He attended University of Peradeniya, Sri Lanka where he was recognized for his academic achievements and service to the Statistics and Computer Science Department and received his Bachelor of Science in Computer Science (First Class Honors) in 2006. Sampath continued his education at Texas State University-San Marcos when he entered the Computer Science Master's program in the spring of 2007. During his time at Texas State, he has pursued an array of research of both biologically and mathematically significant, including research on human oculomotor plant, biometric identification via an oculomotor system and mTBI patient's deficiency in the oculomotor functions. Sampath has been recognized multiple times by Texas State Graduate College, the Computer Science Department, and national organizations for his academic and research achievements in the form of research grants, scholarships, and awards. His research interests are in the area of Brain and Cognitive Science, Computational Neuroscience, Human Oculomotor Plant Modeling, Man-Machine interaction (MMI), and Artificial Life (Alife). He received prestige Sigma Xi grant-in-aid of research grant "twice" for his proposals on 2DOPMM Biometric identification and mTBI patient's deficiency in the oculomotor function.

Sampath currently resides in San Marcos, Texas with his wife Nirmala Karunarathna (molecular biology doctoral student at Texas State University-San

Marcos). In December 2009 Sampath & Nimmi welcomed their son “Pahan (means light) Thiloka (means three worlds) Jayarathna” into the world, who will someday be proud to call Mom and Dad, scientists.

Permanent Address: 28, Pinnagolla Watta, Pahalagama,

Udubaddawa 60250, Sri Lanka

This thesis was typed by Sampath Jayarathna